UNIVERSITY OF CALIFORNIA
RIVERSIDE

Investigation of Brain Computer Interface as a New Modality in Computer Aided Design/Engineering Systems

A Dissertation submitted in partial satisfaction
of the requirements for the degree of

Doctor of Philosophy

in

Mechanical Engineering

by

Ehsan Tarkesh Esfahani

September 2012

Dissertation Committee:

Professor Sundararajan Venkatadriagaram, Chairperson
Professor Thomas Stahovich
Professor Bir Bhanu

The Thesis of Ehsan Tarkesh Esfahani is approved:

Committee Co-Chairperson

University of California, Riverside

Acknowledgment

Foremost, I would like to express my sincere gratitude to my advisor, Prof. Sundararajan, for the continuous support of my Ph.D study and research, for his patience, motivation and moral support.

I am also grateful to Prof. Thomas Stahovich and Prof. Bir Bhanu for taking their precious time being my dissertation committee members. I am extremely thankful to Prof. Thomas Stahovich for his technical suggestions and support throughout my graduate studies at University of California Riverside.

I like to acknowledge National Science Foundation for partially supporting my PhD studies through NSF grant (0729422 and 0935239).

Last but not least, my love goes to my family and friends especially my parents whom without their spiritual supports this dissertation would not be possible.

ABSTRACT OF THE DISSERTATION

Investigation of Brain Computer Interface as a New Modality in Computer Aided Design/Engineering Systems

by

Ehsan Tarkesh Esfahani

Doctor of Philosophy, Graduate Program in Mechanical Engineering
University of California, Riverside, September 2012
Professor Sundararajan Venkatadriagaram, Chairperson

Brain–computer interfaces (BCIs) are recent developments in alternative technologies of human computer interaction. These interfaces aim to interpret the brain's activity as user intentions in active BCI systems or cognitive/ emotional state in passive BCI systems.

This dissertation focuses on implementation of BCIs in different aspects of Computer Aided Design system. Specifically, the dissertation explores the use of BCI in creating, selecting and modifying objects in CAD systems.

Geometry creation is achieved through visual imagery by recording and analyzing EEG signals when subjects imagine distinct shapes. The algorithms developed in this research successfully classified the primitive shape that a subject imagined with an average accuracy of 44.6% (chance accuracy is 20%). The research further indicated that geometrical properties of objects such as roundness and parallel extrusion are also salient in classifying imagined objects.

Selection and modification of objects is obtained by developing algorithms based on the P300 characteristic of the EEG signal and motor imagery. The classification result indicates the proposed method can select the target object/face with an average accuracy of 74%.

Furthermore, the dissertation discusses a method to estimate user emotions of satisfaction and frustration that follow the successful or unsuccessful execution of a user command by the computer. This estimate is derived based on a combination of relative power spectral density and largest Lyapunov exponents. The results show that the algorithms can determine the user's satisfaction level (negative, neutral and positive level) with an average accuracy of 79%.

Content

List of Figures

List of Tables

List of Abbreviations

BCI	Brain Computer Interface
ECoG	Electrocorticography
EEG	Electroencephalography
EMD	Empirical Mode Decomposition
EMG	Electromyography
EOG	Electrooculography
ERD	Event Related Desynchronization
ERP	Event Related Potential
ERS	Event Related Synchronization
fMRI	Functional Magnetic Resonance
fNIR	Functional Near Infrared
HHT	Hilbert-Hunag Transform
ICA	Independent Component Analysis
IMF	Intrinsic Mode Functions
INR	Intra-cortical Neuron Recording
LDA	Linear Discriminant Analysis

LLE	Largest Lyapunov Exponent
MEG	Magnetoencephalography
PET	Positron Emission Tomography
PSD	Power Spectral Density
SSVEP	Steady State Visual Evoked Potential

Chapter 1

Introduction

This chapter presents the motivation and objective of this thesis. An outline of this dissertation is presented in the second section.

1.1 Motivation and Objective

The traditional mouse and keyboard dominate the interfaces for computer-aided design (CAD) systems. However, the emergence of technologies such as pen-based systems, haptic devices and speech recognition software has provided alternative means of interaction [1–3]. These alternatives seek to reduce the number of steps to activate commands for creating or editing CAD models and to obtain faster feedback from users [4].

A more recent commercial technology in human computer interaction is the brain-computer interface. New developments in brain computer interfaces (BCI) have made it possible to use human thoughts in virtual environments [5–7]. BCIs create a novel communication channel from the brain to an output device bypassing

conventional motor output pathways of nerves and muscles. Currently, noninvasive BCIs are based on recording electroencephalography (EEG) signals by placing electrodes on the scalp. Several recent prototypes already enable users to navigate in virtual scenes, manipulate virtual objects or play games just by means of their cerebral activity [8], [9].

This dissertation investigates different applications of brain computer interfaces in CAD environments. The objective of such interfaces is to use the designer's brain activity to create and edit CAD geometry. For a BCI system to succeed as a CAD interface, it must at least allow the basic interactions that a mouse-and-keyboard system (the traditional CAD interface) does. A typical CAD system allows users 1) to create geometrical shapes, 2) to edit shapes by resizing or by operations such as Booleans, sweeps and extrusions and 3) to move shapes by rotations and translations. In addition, a CAD system provides extensive viewing capabilities such as zooms and rotations. In order to operate a CAD system with BCI, the following issues should be addressed:

- Geometry representation: Before designing a 3D geometrical model of an object, a user has a mental representation of the shape. The question is whether it is possible to retrieve information from this visual imagery construct a 3D CAD model. Can the BCI capture the shape and its attributes such as dimensions and proportions accurately enough to generate CAD shapes?

- Geometry editing: Can the BCI be used to edit the shapes that have been created? For example, can it be used to perform Boolean operations, sweeps, or lofts accurately?
- Object manipulation: To edit a design, it is important to move, scale and rotate an object in a desired direction. Can BCIs be used to precisely locate and orient objects?
- Error corrections: Can we get feedback from users' thoughts to correct errors in the model generated by the BCI interface? For example, can we perform an "undo" command by getting emotional feedback or cognitive feedback?
- Training period: How much training data is needed per subject to train different BCI command? Does the training have to start *de novo* for each subject or can we establish baseline classifiers for the various operations that can then be fine-tuned to each user by a customization procedure?

Suppose that a designer wants to create the object shown in Figure 1-1. One scenario of user interaction is as follows: 1) The designer first imagines a cube corresponding to the main body of the object. When the cube appears on the screen, 2) He/she can select one or multiple surfaces for further modification 3) Upon selection of the surface, he/she can edit the object by imagining the movement of selected surface or part in a desired direction (Motor Imagery) 4) Object modification will stop as soon as the user stops motor imagery 5-7) User select another face for modification and shape it to a desired form with motor imagery. 8) User then imagines a negative cylinder corresponding to the hole and imagines its

extent. If the size of the hole is smaller than what he/she needs, he/she imagines increasing the size of the hole till it reaches the appropriate size.

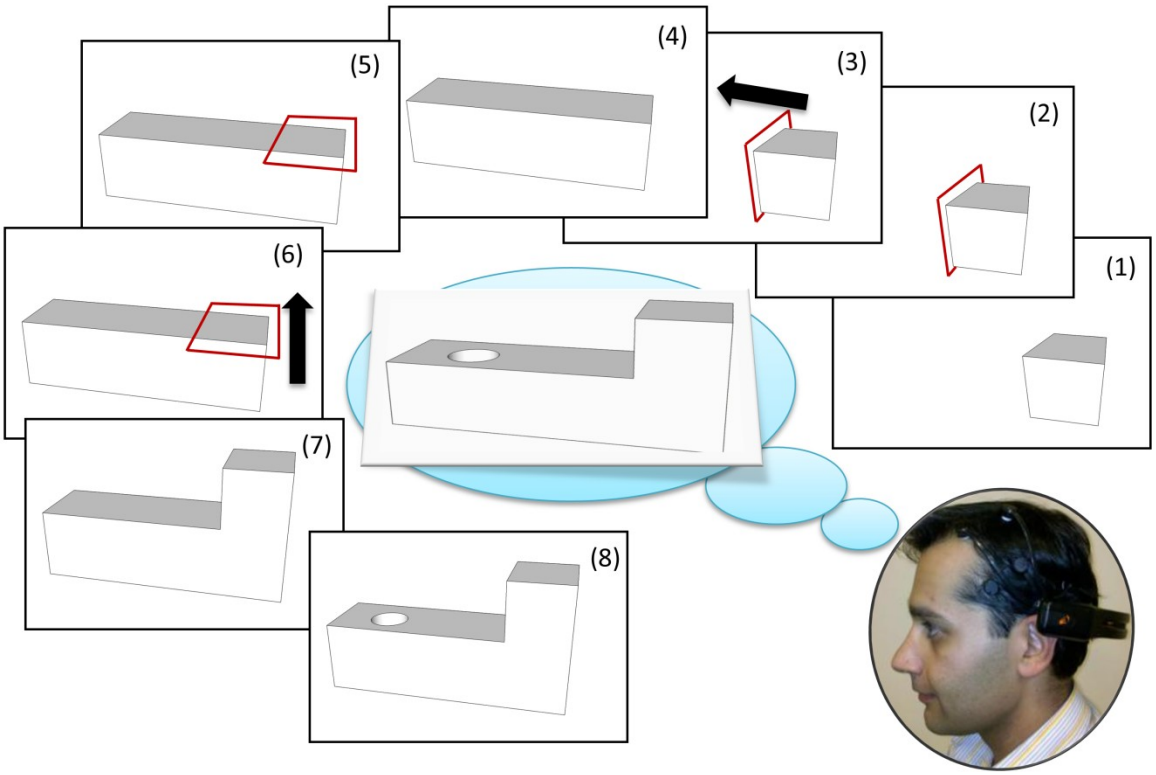

Figure 1-1 An alternative scenario for converting the user's imagined shape into a 3D object via his brain signal

The tasks for the BCI corresponding to the designer's tasks above are:

1) To determine the class of primitive object that the user was thinking about, its overall size and the relative dimensions of its features,
2) To determine the locus of the user's gaze for selecting the desired surface,
3) To interpret user's imagined motor actions and to move or modify the object accordingly,
4) To receive feedback from motor imagery to stop object modification and/ or movement as the shape reaches its desired form,

5) To differentiate between imagery of positive and negative shapes, and

6) To detect user dissatisfaction that result from the computer's misinterpretation of the user's command

Some of these issues such as moving or rotating object via brain signals have been well studied by other research groups. Thus, motor imagery is not a primary subject of this thesis and the state of the art is used as an available tool (See Chapter 6). Other issues such as object creation (visual imagery classification), surface selection and satisfaction are studies in next chapters.

1.2 Outline of Dissertation

This dissertation is organized as follows: Chapter 2 provides a brief background on the current status of brain computer interfaces in CAD. Chapter 3 presents the general structure of translating EEG signal to user's command or feedback and discusses data recording, preprocessing, feature extraction/selection and classification.

Each of chapters 4 through 6 focuses on the implementation of different types of BCI – active, reactive and passive, in CAD systems for geometry generation and selection as well as human's satisfaction detection in interaction with machine.

Chapter 4 investigates the possibility of using BCI for geometry specification. It describes a series of experiments with the following objectives: (i) to explore the feasibility of using BCI to distinguish between five primitive shapes (cubes, cylinders, spheres, cones and pyramids) imagined by the designer (ii) to check the

stability of the results over time (iii) to find characteristic features in EEG signals based on geometrical features of an imagined object.

Chapter 5 explores the use of user's satisfaction in human-computer interaction. The chapter describes an experiment where the user is asked to navigate a robot in a virtual maze. Feature extraction and classification algorithms then estimate the user's emotions of satisfaction and frustration that follow the successful or unsuccessful execution of a user command by the computer.

Chapter 6 introduces a hybrid BCI for object modification in CAD. It describes a real time implementation of a BCI system based on P300 – feature of the EEG signal and on motor imagery. This system enables the user to select and move objects in virtual environments using their thoughts. This chapter discusses a method to select surfaces of an object using the P300 feature and a method to modify objects using motor imagery with SSVEP as internal feedback.

Chapter 7 provides an overall evaluation of BCI as an alternative modality in CAD/E system and discusses the future direction in implementation of BCIs in such systems. It then provides the future prospects of this new modality in design environment.

Chapter 2

Brain Computer Interfaces

Brain-Computer Interface (BCI) technology is an alternative communication channel that enables users to send information via their thought to a computer application. BCI was primary designed for patients with severe neuromuscular disability [10]. However multidisciplinary research and progress in cognitive neuroscience, pattern recognition and signal processing have inspired the use of BCI as a new modality in human-computer interactions. BCIs use brain signals to collect information on user intentions and translates the brain activity as either a cognitive feedback or mental command [11]. For that purpose, two types of brain activities can be used: (i) electrophysiological and (ii) hemodynamic.

Electrophysiological activity is the summation of the electrical potentials of many neurons. When neurotransmitters are released at a synapse, they cause an influx of positive ions that depolarize the neurons which is known as post-synaptic potential (PSP). Each neuron that receives the synaptic input forms a dipole between the soma (cell body) and apical dendrites. The human brain consists of

approximately 100-billion neurons. When thousands of spatially aligned neurons receive similar synaptic input, the summation of their dipoles yields a voltage which can be detected on the scalp [12]. Furthermore, since fluctuating electrical dipoles are associated with magnetic fields, these individual magnetic fields can be added to form magnetic fields which can be detected on the scalp.

Electrophysiological activity in the brain can be measured both invasively and noninvasively. Non-invasive recording includes magnetoencephalography (MEG) where the magnetic field is recorded and electroencephalography (EEG) which records the voltage [13]. EEG uses electrodes placed directly on the scalp to measure the weak (5-100 μV) electrical potentials. The main drawback of this method is a poor signal-to-noise ratio. In order to increase the quality of signal, the recording site should be placed closer to the EEG source. Invasive methods are used for this purpose.

Two invasive techniques for recording electrophysiological signals are the electrocorticogram (ECoG) [14], [15] and intra-cortical neuron recording (INR)[16]. ECoG places a mesh of electrodes on the surface of the cortex, while INR implants micro-electrodes inside the cortex. Both of these techniques provide a very good signal-to-noise ratio. However they have two main draw-backs, 1- they are invasive 2- They cannot cover the whole cortex and therefore they are limited to certain applications [17].

Figure 2-1 compares the invasive and non-invasive BCI for recording electrophysiological activity within brain. Figure 2-1(a) illustrates the voltage based

recording of electrophysiological activity. The recording site are invasive methods (ECoG and INR) are under the skull while EEG electrodes pick up the signal on the scalp. Figure 2-1(b) shows MEG, a non-invasive method that records the magnetic field producing by the dipoles.

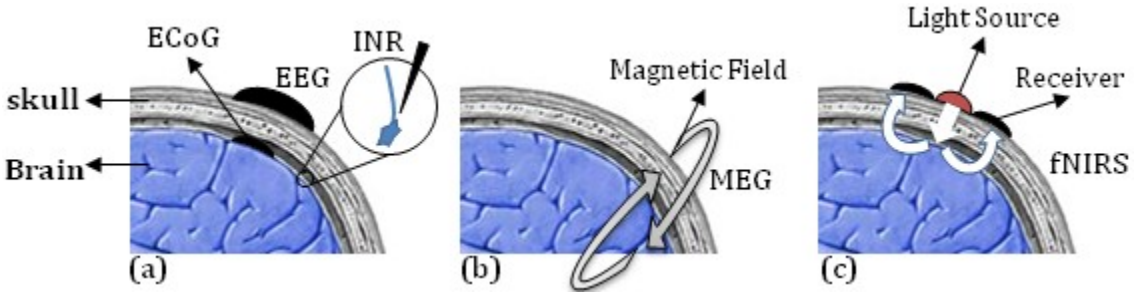

Figure 2-1 The Comparison of different BCI recording

Hemodynamic activity is a process in which a higher rate of blood glucose and oxygen are released to active neurons than inactive neurons. These changes in oxygen blood content can be quantified by neuroimaging methods such as functional magnetic resonance (fMRI) [18–20], Positron emission tomography (PET) [21] and functional near-infrared spectrography (fNIRS) [22]. These methods rely on the blood-oxygen levels at various locations of the brain.

fNIRS technology works by projecting near infrared light into the brain from the surface of the scalp and measuring optical scattering at various wavelengths, which represents localized blood volume and oxygenation changes [23]. This information changes can be used to generate detailed functional maps of brain activity based on the rate of oxygen consumption [22]. The mechanism underlying fINRS is shown, in Figure 2-1(c).

Similarly fMRI and PET use blood-oxygen levels contrast. In fMRI, the difference in magnetization of oxygen-rich and oxygen-poor blood is measured [18]. PET is a radioactive agent-based technique in which fludeoxyglucose (FDG) is used to map neural metabolic activity in terms of regional glucose uptake [17].

fNIRS, fMRI and PET can provide information about phenomena that occur not just close to the scalp but also in deeper structures. These methods also provide better spatial resolution than the EEG as they directly measure activity in different regions. EEG, on the other hand, measures the scalp voltage that could be the result of the addition of voltages from various parts of the cortex. However, fNIRS, fMRI and PET share the drawback of having a low temporal resolution, since it takes 2-5 seconds to detect the change of local blood flow in response to neural activity. The spatial resolution of fNIRS is also low; its greatest potential therefore lies in being a secondary measure to provide additional information on brain activity through the BOLD component. Figure 2-2 compares the spatial and temporal resolution of discussed methods.

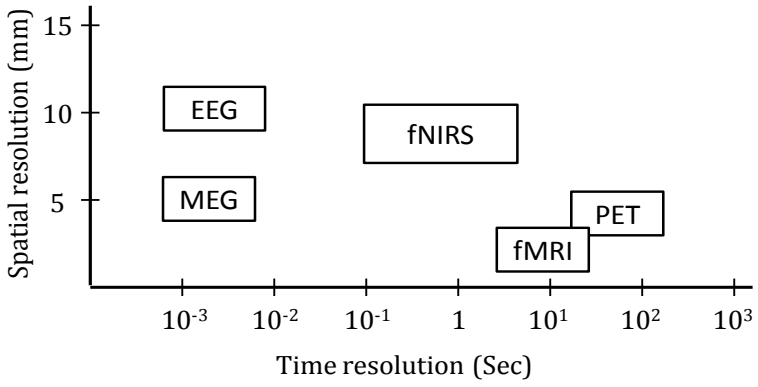

Figure 2-2 Comparison of spatial and temporal resolution of different brain imaging techniques

Among the current monitoring methods, EEG constitutes an attractive choice for BCI systems because it is non-invasive and relatively simple to implement. Furthermore, recent advances in wireless systems and electronics have made the EEG relatively inexpensive as well. Therefore, most BCI researchers focus on EEG-based systems. Thus, throughout this dissertation, BCI will stand for EEG-based BCI.

Based on the type of information and technology that is used to extract them, BCI systems can be categorized as *active*, *reactive* and *passive* systems [24].

- *Active BCI*: In an active BCIs, the user, voluntarily and independent of external events, starts a mental task to generate commands to external applications. Motor imagery is the best example of active BCI.
- *Reactive BCI*. In reactive BCIs, the brain's reaction to an external stimulus generates the output command or feedback. Reactive BCIs are indirectly modulated by the user for controlling an application. Applications based on visual evoked potentials and P300 are the best examples of reactive BCI (See Section 2.2.1 and 2.2.2).
- *Passive BCI*. A passive BCI outputs a cognitive feedback from user's mental state from his/her arbitrary brain activity without any voluntary control. Level of engagement, excitement, and workload are some of the examples of cognitive feedbacks in passive BCI.

2.1 Active BCI

In active BCIs, the user voluntarily generates specific patterns of brain activity which can be detected by a machine learning algorithm, so that the resulting information can be used as a real-time input modality for controlling a device by thought. Some examples of active BCI systems are motor imagery [13], [25–27], visual imagery [28], [29] and other mental task such as auditory imagery of music and spatial imagery involving navigation in familiar surroundings [30]. Among the various mental tasks that have been studied, motor imagery has been the subject of most BCI because motor imagery has the potential to open a new communication channel for disabled individuals. Visual imagery also plays an important role in human computer interactions. The next sections provide more information on these tasks.

2.1.1 Motor Imagery

Functional brain imaging studies have shown similar patterns of activity during motor imagery and actual movement performance [31]. This similarity makes motor imagery a good mental task for BCIs [32].

Motor activities such as movements of hands and fingers are associated with the mu-rhythms of the EEG that can be recorded at sensorimotor cortex [25], [31]. The mu-rhythms have three primary frequency components: a component between 9-11 Hz, a component near 20 Hz and one near 40 Hz.

Sensorimotor stimulation, motor behavior, and mental imagery can change the functional connectivity within the cortex and result in amplitude suppression known as event-related desynchronization (ERD) or in amplitude enhancements refereed to event-related synchronization (ERS) in certain frequency components (alpha and central beta) [31]. Preparation and planning of self-paced hand movement results in a short-lasting ERD of the alpha and central beta rhythms [31], [33]. This is followed by ERS upon completing actual/imagery movement and with relaxation.

BCI research groups have used motor imagery tasks such as left-right hand movement [34], [35] and foot movement [36] and have implemented them for navigation in virtual systems [37] or cursor movements [38].

2.1.2 Visual Imagery

Visual imagery is the set of processes associated with "seeing" with the mind. The goal in using visual imagery in BCI is to explore whether the entire object or certain characteristics of the object can be detected from the user's EEG signal when he/she imagines the object. The following two different models are often tested in this regard:

- Property based models: These models seek to find specific attributes of the object that define the object. For example, sensory features such as the form and color of the object or the typical motion of the object may be used as attributes. Other attributes may be functional/verbally mediated properties such as where an object is typically found, its social significance, etc. [39].

- Domain specific models: These models classify objects based on their domains. For example, human faces, buildings, animals, and man-made objects are assumed to belong to different domains.

Domain specific model has been widely investigated in the classification of visual imagery. Reddy et al. [40], using fMRI, were able to classify different categories of imagined objects when they presented participants with auditory prompts of four categories of objects –food, tools, familiar faces and buildings and asked them to mentally construct visual images of these objects. A similar study has been conducted with EEG analysis in the form of event related potentials (ERP) by Simanova et al. [41]. They used multivariate pattern analysis to classify EEG data recorded during visual imagery of faces, plants and tools and could achieve accuracies of 89% with object drawings as visual cue. They also used auditory and orthographical cue which results in a lower, though significant, classification accuracy.

Furthermore, Bobrov et al. applied categorical object-based classification of single trial EEG to distinguish between face, buildings and animals during visual imagery [28]. They used common spatial pattern to extract features from PSD of different frequency bands. Using a Bayesian classifier, they achieved an average classification rate of 58% over seven subjects. The information transfer rate of their system was in average 29 bit/min with a maximum of 35 bit/min.

2.2 Reactive BCI

In reactive BCI, the signal of interest is the brain response to an external stimulus. External visual or auditory stimuli elicit EEG signals. These signals have specific characteristics in time and frequency domain which depend on the task and the way the stimulus is presented. The most prominent example of a reactive BCI is the P300 speller [42], [43]. Other examples include also BCIs based on steady state visual [44–46], somatosensory [47], [48] or auditory potentials [49].

2.2.1 P300

P300 is a positive EEG peak that occurs during 200–700ms (typically 300 ms) after stimulus onset, and is typically recorded over the central-parietal scalp [50]. The response is evoked by attention to rare stimuli in a random series of stimulus events (i.e., the oddball paradigm).

In P300-based BCIs, the subject is presented with a sequence of events that can be classified into two categories: target and non-target. The task of the subject is to focus on target events that occur less frequently. As a result, a prominent P300 component will be appear in ERP signal which can determine the subject's intent.

The first P300 based BCI was P300 speller designed for locked-in patients [51]. All alphabets were placed in a 6x6 matrix after which its rows and columns were randomly flashed. P300 component would be detected after the flash of the row or the column on which the target letter was.

2.2.2 Steady State Visually Evoked Response

A steady-state visual evoked potential (SSVEP) is a resonance phenomenon arising mainly in the visual cortex when a person is focusing his/her visual attention on a light source flickering with a frequency above 6 Hz [52]. An SSVEP can be detected by examining the spectral content of the signals in the visual cortex. When actions are associated with target flickers of different frequencies, the subject can control a BCI by gazing at the target corresponding to the desired action.

Different versions of cursor movement have been implemented by using SSVEP [44], [53–55]. Usually multiple directions are marked by small flickering squares on the display, each one flickering at a slightly different frequency. When the user gazes at the desired flickering bar, the frequency component of the flashing object can be detected in the frequency spectrum. SSVEP applications do not need training period and are often detectable by using a threshold in frequency domain.

2.3 Passive BCI

The main purpose of passive BCI is to gain information about the ongoing user state, including involvement, work load and emotions. As emotion and satisfaction are encoded in human cognition, passive BCI may also be referred to as cognitive monitoring [56]. The outcome of this type of BCI can be used to give a situational evaluation of a human interaction, which can be utilized for neuro-ergonomics, usability tests or a user state detection related to experimental conditions [57], [58].

Novel systems based on passive BCIs can detect or even predict error potentials [59–61].

Chapter 3

Experimental methodology

EEG-based systems share the same fundamental steps in EEG signal processing and classification which are shown in Figure 3-1.

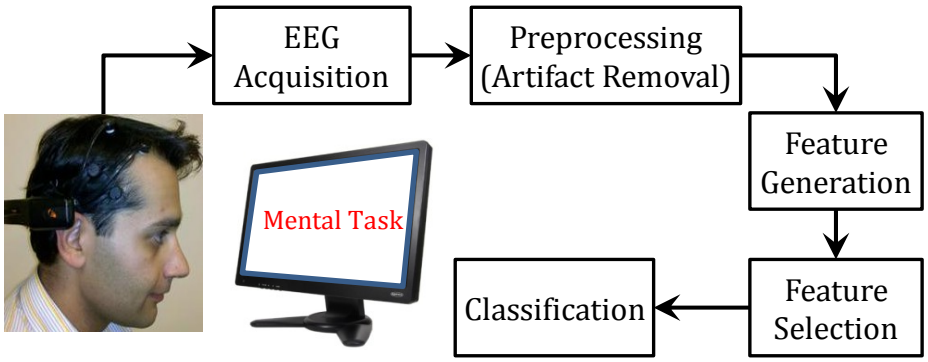

Figure 3-1 Process of developing BCI for translating EEG signals

The recorded brain signals include artifacts such as muscle movement, eye movement, etc. The goal of the preprocessing step is to remove the artifacts from the EEG signals. The feature generation and selection blocks in Figure 3-1 transform the preprocessed signals into a feature vector. The generated feature vector should have statistically significant differences for different classes of imagined objects. The classification block uses the feature vector to classify an unknown event based

on a set of observed events (training data). The details of each of these blocks are explained in next subsections.

Feature extraction depends on the BCI category (active, reactive or passive) and on the mental task required in the experiment. The following sections introduce the data acquisition, preprocessing methods and classification that are common in all the EEG experiments performed in this study. Feature extraction/selection specific to each experiment will be described in its related chapter.

3.1 Data Acquisition

EEG signals are recorded using the Emotiv neuroheadset [8] at 14 channels (plus CMS/DRL references, P3/P4 locations). The channel names based on the international 10-20 locations are: AF3, F7, F3, FC5, T7, P7, O1, O2, P8, T8, FC6, F4, F8, AF4, which are indicated in Figure 3-2.

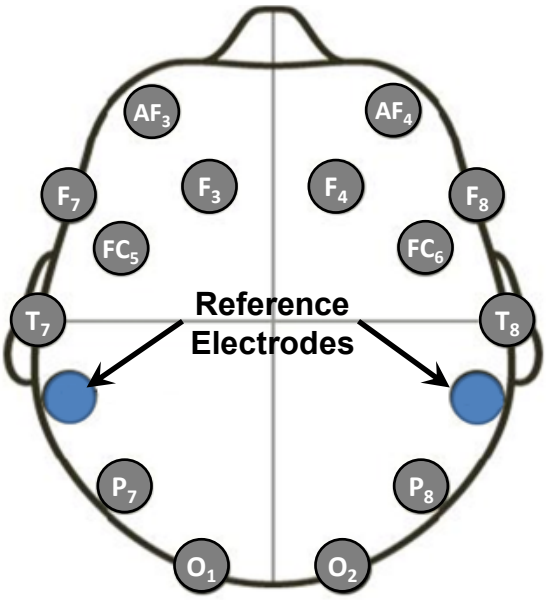

Figure 3-2 EEG Recording location

3.2 Signal Conditioning and Artifact Removal

The main artifacts in EEG signals are muscle movements –Electromyography (EMG)- eye blinks and eye movements –Electrooculography (EOG).

Figure 3-3 shows the domain of each signal in amplitude and frequency. It can be seen from Figure 3-3 that a simple low pass filter around 30 Hz can remove most of EMG artifacts. Therefore the main concern in artifact removal is EOG and eye blinks.

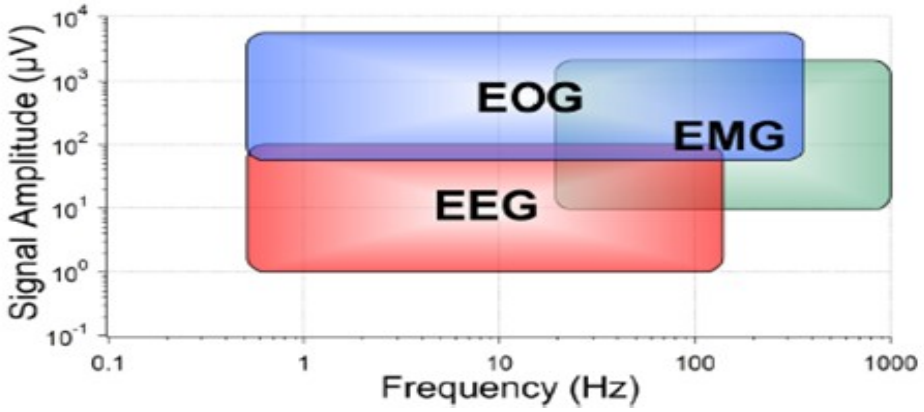

Figure 3-3 EEG and its artifact

The recorded EEG data at each channel is the difference between the potential from a source to the channel location and the reference electrodes. The recorded EEG signals $\{X = x_1(t), x_2(t), \ldots x_{14}(t)\}$ can be assumed to be a linear combination of '*n*' unknown and statistically independent sources $\{S = s_1(t), s_2(t), \ldots s_n(t)\}$ (Figure 3-4). In other words, *X=WS* where '*W*' is a weighting matrix. Since we record the signals at 14 channels, we assume that there are 14 independent sources too (n=14).

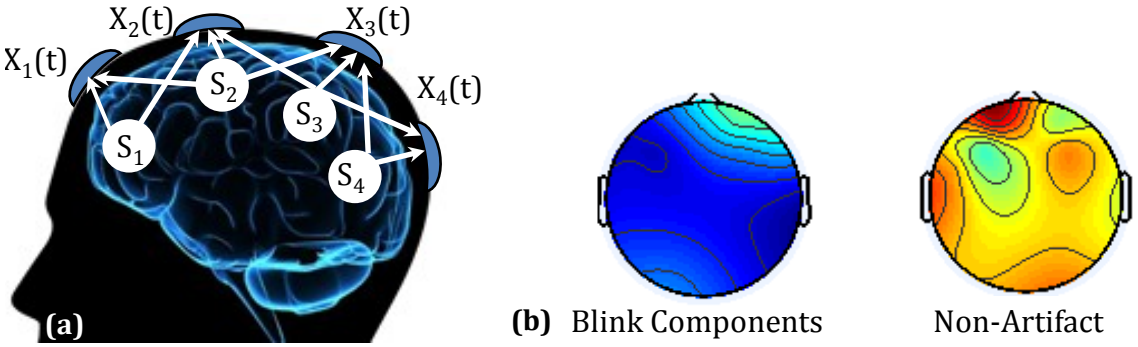

Figure 3-4 A) Blind source separation of EEG signals through ICA B) Brain map and of an IC associated with blink artifact used as a template

In the preprocessing step, a combination of independent component analysis (ICA) and empirical mode decomposition (EMD) is used to detect and remove artifacts. It has been shown by Onton and Makeig [62] that independent components of EEG signal represent synchronous activity in underlying cerebral and non-cerebral sources (e.g., potentials induced by eye or muscle movement) and therefore can be used to separate the artifact signal from the cerebral activity.

The main aim of ICA step is to find the independent components of the recorded data in each trial, such that they have the minimum mutual information [62]. In other words:

$$S_X = W^{-1} X \qquad \text{where} \qquad S_X = [s_1(t), s_2(t), \ldots s_n(t)] \qquad (3\text{-}1)$$

The weighting matrix '*W*' can be found by minimizing the mutual information $I(S_X)$ between the sources, S_X, given in Equation (3.2)

$$I(S_X) = \int p(S_X) \log \frac{p(S_X)}{\prod_{i=1}^{n} p(s_i)} ds \qquad (3\text{-}2)$$

Where $p(.)$ denotes the probability density of the argument. To implement ICA decomposition, we use the logistic infomax ICA algorithm [63], [64] with natural

gradient and extended ICA extensions implemented in EEGLAB by Delorme and Makeig [64]. After performing ICA decomposition, independent components '$s_i(t)$' associated with artifacts like eye blink or muscle movement are detected based on their signature on brain maps and power spectral density method [62], [66]. Figure 3-4b compares the brain map of a blink–related component to a normal one. It can be seen that, in blink-related component, there is a strong far-frontal projection typical of eye artifacts.

EEG signal is usually corrected by removing the artifact related IC. However, one of the limitations of ICA is that the ICs selected for removal contain not only ocular activity but also some EEG activity, especially when the number of recording electrodes is relatively small (14 electrodes in our case). Therefore, straightforward removal of these ICs might lead to a loss of EEG data. Thus, after detection of artifact related IC, we use empirical mode decomposition (EMD) to clean it as proposed by Lindsen and Bhattacharya [67]. This process is shown in Figure 3-5.

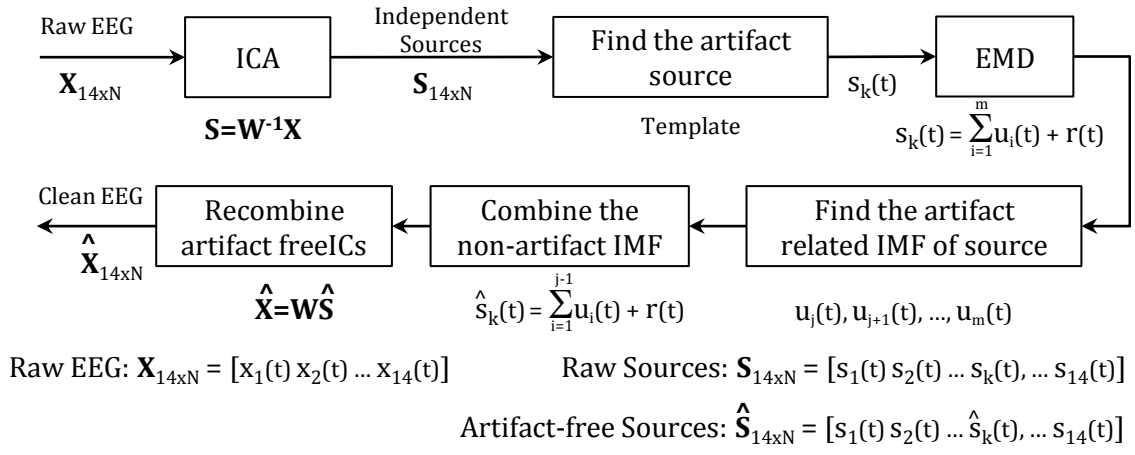

Figure 3-5 ICA-EMD Combination for artifact removal

EMD decomposes the artifact-contaminated IC signal into a finite set of intrinsic mode functions (IMFs), and then uses a threshold to detect and remove the artifact related component in the contaminated IC. Therefore, by summing up the non-artifact components in the artifact related IC, that independent component can be cleaned. Finally, the artifact free EEG can be obtained by using the artifact free sources in Equation 3.1.

Intrinsic Mode Functions (IMFs) are defined as a class of functions that satisfy two conditions:

1- In the whole data set, the number of extrema and the number of zero crossings must be either equal or differ at most by one. (In other words, every adjacent local maxima and minima must across the zero line.)

2- At any point, the mean value of the envelope defined by the local maxima and the envelope defined by the local minima is zero. (In other words, the upper envelope and the lower envelope estimated from the local maxima and local minima are approximately symmetric with regard to the zero line.)

To extract IMFs from the artifact contaminated source signal *S(t)*, empirical mode decomposition uses a sifting process which is demonstrated in Figure 3-6A.

As each IMF $u_i(t)$ is extracted, it is subtracted from the original signal to define the residue $r_i(t)$. Since the residue still contains information related to longer period components, sifting process will be applied to it again to extract a new IMF. This process is shown in Figure 3-6B. It will be stopped when either the residue

becomes a monotonic function or its amplitude gets too small that can be considered inconsequential.

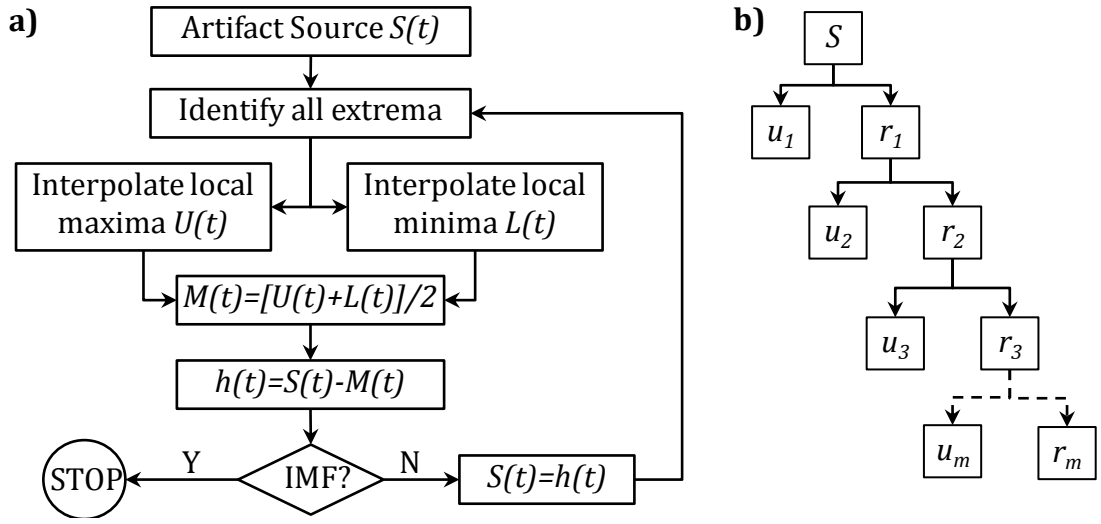

Figure 3-6 A) Siftting method for finding each IMF. B) Empirical Mode Decomposition of the signal to m IMF

Using the EMD method, the artifact related source *S(t)* is represented as a sum of n IMFs $u_i(t)$ and a residue r as shown in Equation 3.3.

$$S(t) = \sum_{i=1}^{m} u_i(t) + r \qquad (3\text{-}3)$$

The next step in artifact removal process is to determine which IMFs of artifact related component are related to eye movement.

As shown in Figure 3-3, EOG components have low frequencies and large amplitudes. Therefore, IMFs with EOG components will have a larger standard deviation (SD) than EEG related IMFs. The IMFs are sorted in descending order of frequency - $u_1(t)$ associated with the locally highest frequency and $u_n(t)$ with the lowest frequency. Based on this property, it is suggested by Lindsen and

Bhattacharya [67] that if the SD of an IMF is larger than 1.5-2 times the SD of the first IMF, then that IMF is a blink-related component. By removing the artifact-related components, the related IC can be cleaned and ultimately the eye movement/blink artifact can be removed from the EEG signal. This procedure is shown in Figure 3-7, where IMF of an independent component associated with artifact are detected and removed to clean the raw EEG signal.

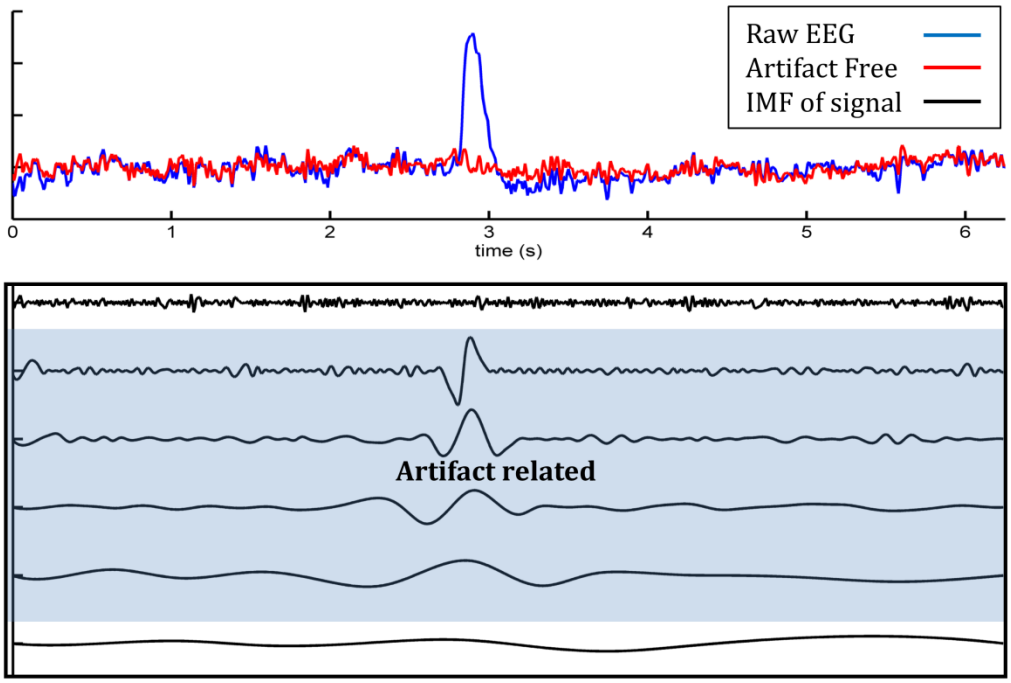

Figure 3-7 Contaminated EEG and its artifact component in its intrinsic mode functions, Artifact related components are highlighted

3.3 EEG Components for Feature Extraction

The selection of feature extraction methods depends on the BCI category (active, reactive or passive) and on the mental task required in the experiment. The features of interest are usually derived with time series analysis methods such as autoregressive or with frequency analysis of EEG components. In this section, we

give an overview the characteristics of different frequency component of EEG signal which will be later used in Chapter 4 and 5.

The usual classification of EEG rhythms based on their frequency ranges is as follows: delta (1 to 4 Hz), theta (4 to 8 Hz), alpha (8 to 13 Hz), beta (13 to 30 Hz), and gamma (higher than 30 Hz). The alpha rhythm, discovered by Hans Berger in 1929, is typical of a resting condition and disappears when the subject receive a sensory signal or when he/she makes mental efforts [68].The theta rhythm usually appears in periods of emotional stress and during rapid-eye movement sleep [68]. The delta is the dominant frequency band during deep sleep and anesthesia, and is also present during various meditative states involving willful and conscious focus of attention in the absence of other sensory stimuli [68]. The beta rhythm is typical of periods of intense activity of the nervous system and occurs principally in the parietal and frontal regions [68]. Finally gamma band is thought to be associated with attention, perception, and cognition [68].

3.4 Classification

There are different linear and nonlinear machine learning methods such as LDA, SVM, and Neural-Network which can be implemented for classification of EEG signals. Lotte et al. have reviewed a complete list of classification method used in BCI [69].

Among the various classifiers, in this dissertation, we use linear discriminator analysis (LDA) to classify the EEG data into the different categories. LDA has a very

low computational requirement which makes it preferable in this study. The aim of this technique is to find a hyperplane to separate the data from different classes. In a binary classification case, the side of the hyperplane that the feature vector is placed determines the classification result. We have used a multi-class LDA for classification purposes according to the following procedure:

Suppose that the number of classes is *C* and that for each class, the number of training samples is *E*. For each of these training samples, we extract *F* features. Let ${}^{c}f_{i}^{e}$ be the i^{th} feature of the e^{th} example in the training set of class *c*. The sample estimate of the mean feature vector per class is given by:

$$ {}^{c}\bar{f}_{i} = \frac{1}{E}\sum_{e=1}^{E} {}^{c}f_{i}^{e} \tag{3-4} $$

The sample estimate of the covariance matrix of class 'c' is ${}^{c}\Sigma$.

Then the covariance of all classes are averaged to calculate an estimate of the common covariance matrix 'Σ'. Finally the weight associated to each of the features is calculated as:

$$ {}^{c}w_{j} = \sum_{i=1}^{F} \Sigma^{-1}.{}^{c}\bar{f}_{i} \quad 1 \le j \le F; \quad {}^{c}w_{0} = \frac{-1}{2}\sum_{i=1}^{F} {}^{c}w_{j}.{}^{c}\bar{f}_{i} \tag{3-5} $$

For each testing data, a score of classifying as class 'c' is calculated by using Equation 2-5.

$$ {}^{c}score = {}^{c}w_{0} + \sum_{i=1}^{F} {}^{c}w_{i}.{}^{c}f_{i} \quad 0 \le c \le C \tag{3-6} $$

The output of the classification stage for each data set is the class with the highest corresponding score calculated through Equation (3-6).

Chapter 4

Visual Imagery

Mental imagery is defined as "an experience that resembles perceptual experience, but which occurs in the absence of the appropriate stimuli for the relevant perception" [70]. Mental imagery arises when perceptual information is recalled from memory or from previous perceptual input [71]. For every type of perception, there is a corresponding type of imagery. Visual mental imagery ('seeing with the mind's eye'), auditory imagery and kinesthetic imagery - commonly called 'motor imagery'- are the main categories of mental imagery that are be considered in brain-computer interfaces [72].

Motor imagery has been the primary focus of most BCIs [73–78]. Here, signals are obtained during imagined motor responses. For example, Brunner et al. [73] classifies imagined movements of the right and left limbs. Kubler et al. [74] use BCI to capture desired motor movements for patients that suffer from paralysis. Lemm [75] describe a system to classify imaginary hand movements using the μ-rhythm (8-13 Hz) EEG signals. It has been shown that using EEG based BCI, it is possible to

control the 2D motion of a cursor [76–78] and to rotate an imaginary object along various axes [79], [80].

Visual imagery can be classified into two subcategories: object-based imagery (e.g. imagery of shapes and colors) and spatial imagery (such as location and spatial relations) [81]. During visual mental imagery, neural representations of a visual entity are re-activated endogenously from long-term memory and maintained in visuo-spatial working memory to be inspected and transformed [81], [82].

Visual mental imagery consists of two main stages: 1) image generation 2) image maintenance [71]. It has been estimated that the average duration of generated image is about 250 ms [83]. Thereafter, another mental mechanism (image maintenance) is involved in keeping the internal representation of generated image. The neural processes underlying each stage are still unclear. However, fMRI studies have shown that the middle-inferior temporal region of the brain, especially that of the left hemisphere, is involved in image generation [84]. Another study by Mellet et al. [85] reported activity in right occipital cortex during generation-maintenance of the mental image. Cornoldi et al. [86] identified six fundamental characteristics which affect the vividness of mental image or, in other words, the maintenance of mental images. These characteristics are: specificity, richness of detail, color, saliency, shape and contour and context. Although the individual contributions of each characteristic vary, shape and contours are shown to be the best predictors of vividness [87].

Visual imagery has been mostly studied with PET or fMRI rather with than EEG analysis, because EEG signals have a poor spatial resolution that makes it difficult to detect detailed visual imagery. However, even though exact geometry may be difficult to detect, it may be possible to determine the features of the geometry such as roundness, sharpness, symmetry and curvature from the EEG signals [88]. Since the selected objects in this study - cubes, cylinders and spheres, differ in these and other features, the hypothesis of this research is that these primitive geometries can be distinguished from each other using EEG signals when the user imagines these geometries

4.1 Classification of Primitive Shapes

The experiments were conducted as a series of trials. Each trial had two parts. In the first part, the stimulus was presented to the participant; in the second part, participants imagined the object (Details of the experiments are presented in the next section). Figure 4-1 shows the signal recorded in two trials at channel O2.

The first 10% of the signals recorded during the mental task was removed and the rest was used for processing. The EEG signals recorded between the trials were used as baseline. Let E_i, B_i and X_i be the truncated data, baseline and the combination of two during the ith trail (Figure 4-1). For preprocessing, we used the combined signal X_i whereas for feature extraction, we analyzed E_i and B_i separately.

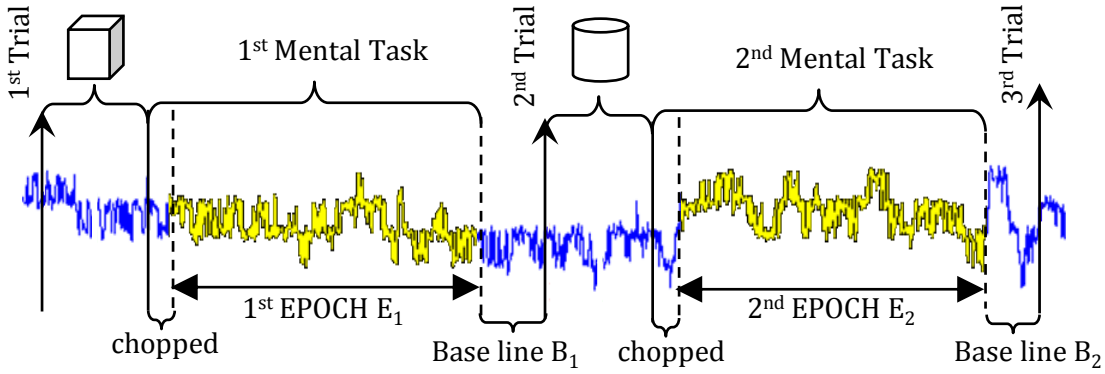

Figure 4-1 EEG signals recorded at channel O_2 and time course for two trials

4.2 Feature Extraction

After removing the artifacts from the EEG signals, we perform another ICA on the artifact free signal $\hat{X}$. This procedure results in 14 independent components { $IC_{\hat{X}} = ic_{1\hat{X}}(t), ic_{2\hat{X}}(t), ...ic_{14\hat{X}}(t)$ }. The new components represent non-artifact sources with minimal mutual information. Then, we divide each component into two segments: the EPOCH component IC_E and the base line component IC_B. We use these components to extract the features.

Several features have been used in the literature for classifying EEG data in BCI for different mental tasks. Some of these features are: band powers [89], power spectral density values [6], [73], autoregressive and adaptive autoregressive parameters [90], time frequency features [91] and inverse model-based features [69]. EEG signals are nonlinear and non-stationary i.e. they may rapidly vary over time and especially over sessions. To deal with this characteristic of EEG signals, we have selected the Hilbert-Huang transform (HHT) over classical time–frequency analysis methods [92].

HHT adaptively tracks the evolution of the time–frequency in the original signal and provides detailed information at arbitrary time–frequency scales. HHT is computed in two steps:

1) Empirical mode decomposition (EMD)

2) Hilbert spectral analysis.

HHT uses the EMD to decompose a signal into a finite set of intrinsic mode functions (IMFs), and then uses the Hilbert transform of the IMFs to obtain instantaneous frequency and amplitude data. Using the EMD method (described in section 3.2), a time series signal $x(t)$ is represented as a sum of *n* IMFs $u_i(t)$ and a residue *r*. Having obtained the IMFs using EMD method, we apply the Hilbert transform to each IMF component. Instantaneous amplitude $\alpha_i(t)$, phase $\theta_i(t)$ and frequency $w_i(t)$ can be expressed as Equation 4-1 to 4-3.

$$\alpha_i(t) = \sqrt{u_i^2(t) + H\{u_i(t)\}^2} \tag{4-1}$$

$$\theta_i(t) = \arctan\left(\frac{H\{u_i(t)\}}{u_i(t)}\right) \tag{4-2}$$

$$\omega_i(t) = \frac{d\theta_i(t)}{dt} \tag{4-3}$$

where $\mathrm{H}\{u_i(t)\}$ is the Hilbert transform of the IMF. The frequency-time distribution of the amplitude over different IMFs is designated as the Hilbert spectrum $\mathrm{H}(\omega,t)$. Finally, the marginal spectrum is computed as Equation 4.4:

$$h(\omega) = \int_0^T H(\omega,t)dt \tag{4-4}$$

Using the Hilbert marginal spectrum, we calculate the power of five frequency bands (Delta1-4 Hz, Theta 4-8 Hz, Alpha 8-12 Hz, Beta 12-30 Hz, Gamma 30-64 Hz) for each independent component of the EEG signals. This results in 70 features per trial (5 power bands for each of the 14 independent components).

Finally, since the total energy of the recorded data can change in time, we normalize the features of each trial with respect to the features of baseline of the same trial. Figure 4-2 shows the steps involved in preprocessing and feature generation.

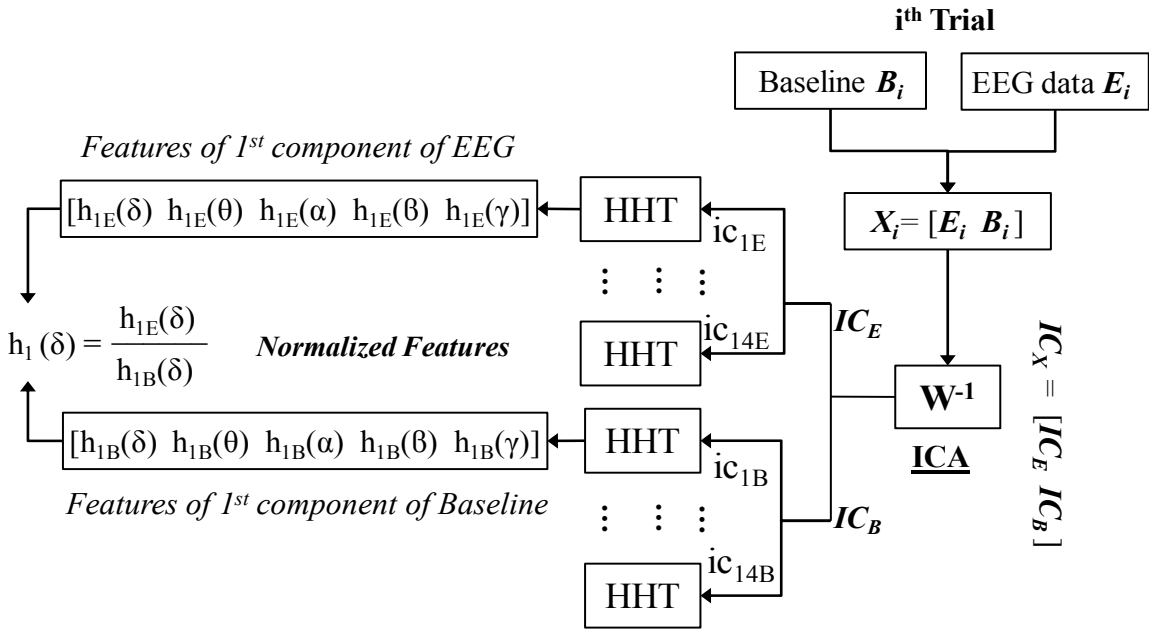

Figure 4-2 Block diagram for Feature generation

4.3 Experimental Study 1: Classifiability

The first experimental study consisted of 10 subjects (7 male and 3 female) between the ages of 18 and 36. All the subjects had a background in engineering but

no experience with brain computer interfaces. The experiment was run in three sessions. Each session lasted 15-20 minutes. There was a break of 5 minutes between sessions 1 and 2, and a break of 15-25 minutes between sessions 2 and 3. Subjects were instructed to notify the experimenter if they experienced fatigue or needed a break at any time during the experiment. The experimental studies were approved by the institutional review board (IRB) of the University of California, Riverside.

In the first session, an image of one of the primitive objects (cube, cylinder, sphere, cone and pyramid) was displayed in a random sequence on the screen for 2 seconds. The images were presented in isometric view at the same location on the screen. They also had the same overall size and color. After this period, the screen went blank and the participant was instructed to imagine the same object on the blank screen at the same location and orientation. The subject was given 5 seconds for the imagery during which EEG data was recorded. At the end of each trial, a message appeared on the screen asking the subject to get ready for the next trial. The interval between each trial randomly varied between 2 and 5 seconds. Each session consisted of 10 trials per object.

In the second session, instead of using the image of an object, a word (e.g. “cube”) appeared as a verbal cue. The reason for this change of type of cue is as follows: Using only visual image cues followed by visual imagery, it would be difficult to tell if the EEG signals are a result of the imagery or just a remnant of visual perception. However, using a different type of cue such as the name of the

object instead of its image can help gain more confidence in the algorithms. If the classifier trained on imagery prompted by visual image cues can perform well on the imagery prompted by verbal cues, then we can be more confident that the classifier is indeed capturing visual imagery. The cues in the third session were the same as first one. However, in this session, each subject performed object imagery of ten simple and ten complex objects shown in Figure 4-3.

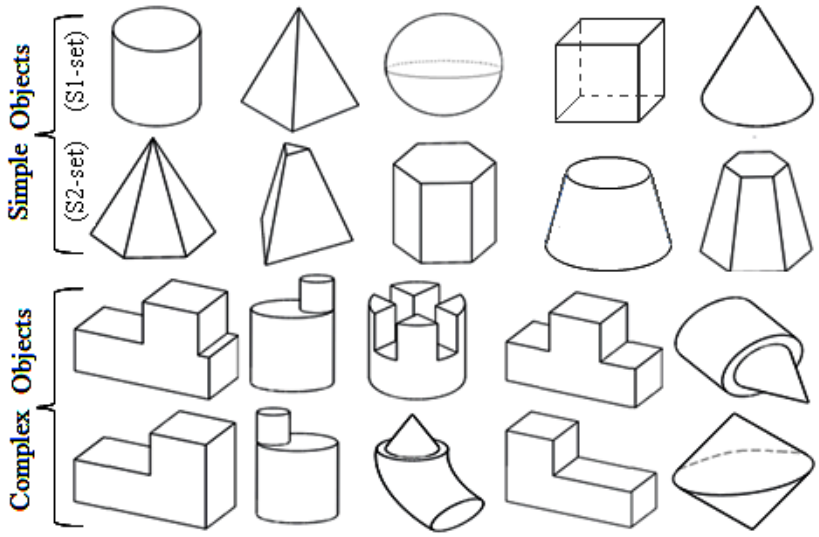

Figure 4-3 Simple and complex objects used in the third session as visual cue

Simple objects are categorized into two sets: 1) five primitive shapes which were used in the first two sessions and we will refer to them as S1-set, 2) five new shapes which were only presented in session 3 (S2-set). The second sets of simple objects were either incomplete versions of the first set (e.g. truncated cone instead of a standard cone) or the same objects with more edges (e.g. hexagonal pyramid instead of a triangular pyramid). The last set of recorded data was complex objects, which were considered as a combination of two or more primitives (Figure 4-3).

4.4 Classification of Primitive Shapes

To classify the primitive shapes, we use a subject-based classifier. Prior to classification, it is important to determine which of the extracted features provides the most useful information about the mental task for each subject. To do so, we used a series of binary feature ranking using the Mann-Whitney-Wilcoxon (MWW) test. 50% of the recorded data for the S1-set of shapes are randomly selected as a training set in feature selection. We rank the features of the training data by MWW test in five binary evaluations (each imagined geometry vs. the other classes). Thus, five rankings for features are obtained, each of which represents the most important features of its corresponding class. The top 3 features of each class are selected as the feature set. Moreover, if any other features appear frequently (in 3 out of 5 ranking) as next top 5 features, it is also included in the feature set.

The MWW test ranked beta and gamma activity at channel location AF4, FC6, P8 and O2 (see Figure 3-2) and theta band at channels O1 and O2 to be among the top features.

Figure 4-4 shows the mean activity of the brain in five frequency bands over 30 trials for subject 5 for each of the five classes. In accordance with the results of the MWW test, Figure 4-4 shows that the right hemisphere is more active during mental imagery-maintenance. These results are also consistent with the findings of Mellet et al. [85].

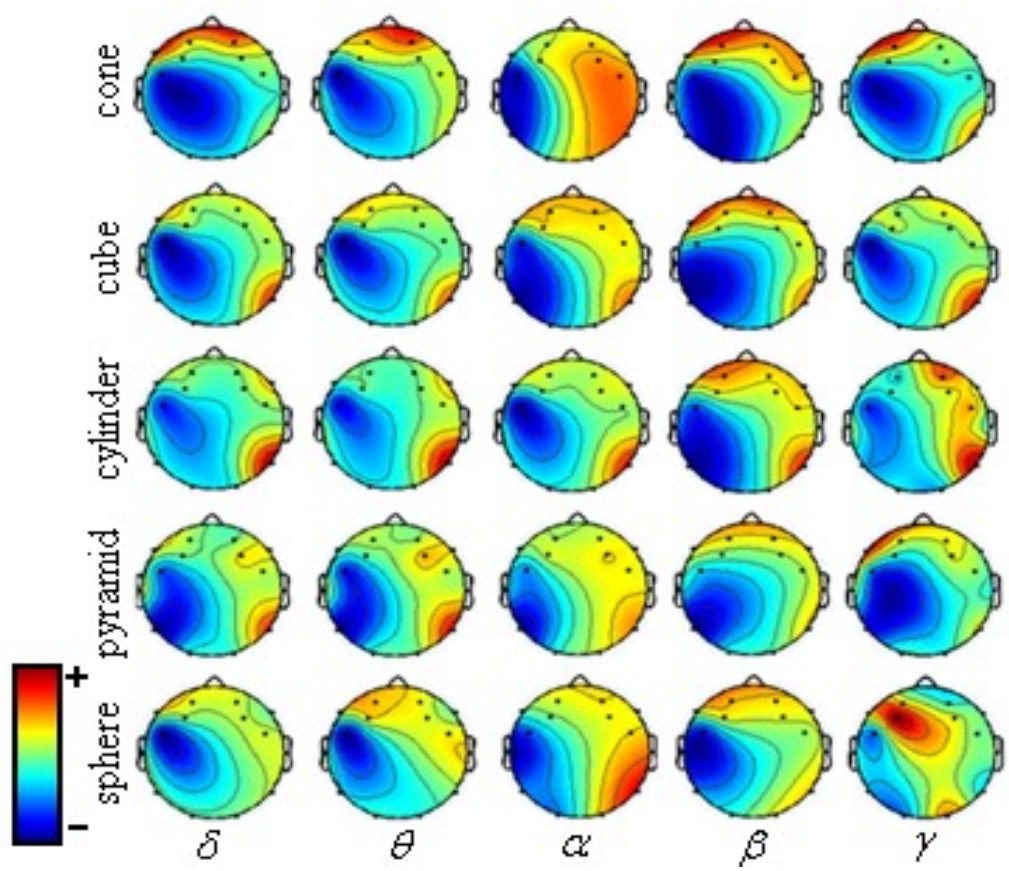

Figure 4-4 Band based map of brain activity for subject 1 during visual imagery of different objects

We perform a subject-based classification within and between different sessions of the same stimulus (image) or different stimuli (text vs. image). In all evaluations, we use a LDA multi-class classifier. The performance of each classifier is evaluated through a 10 fold validation. The average of the classification results for each subject along with information of training and testing sets are given in Table 4-1.

Table 4-1 shows that if 80% of the recorded data is used for training, the average accuracy among the entire subject is about 44.6% (chance accuracy is 20%) which is more than double the expected accuracy of a naïve classifier.

The third row of Table 4-1 shows the robustness of the feature extraction and classification where training and testing data are recorded in two different sessions with a 30~50 min time gap between them. Note that the accuracy of the classifier does not decrease significantly from the first evaluation where the same amount of training data was used.

Table 4-1 Subject based Classification rate for three different conditions

Data set information	S_1	S_2	S_3	S_4	S_5	S_6	S_7	S_8	S_9	S_{10}
Training:50% of sess.1&3-50 image **Test:**50% of sess. 1&3-50 image	38.6	40.9	38	34.8	34	44.9	27.9	38.5	29.4	34
Training:80% of sess. 1&3-80 image **Test:**20% of sess. 1&3-20 image	50.5	43.1	51.6	48	37.1	54.1	35.8	45.8	36	44
Training:sess.1-50 image **Test:** sess. 3-50 image	34.5	40	34	32.5	30	42.5	27.5	36	29.5	31
Training:50% of all sess.-75 image& txt **Test:**50% of all sess-75 image &txt	34.9	38.7	36.5	34.7	32	38	26	34	29.3	30
Training: All sess.1&3-100 image **Test:** All sess. 2-50text	38.7	40	41.2	44	33.4	56.7	26.5	44	32	42.5

To test the robustness of the classification to the stimulus type, both image and text cues are used. The last row in Table 4-1 shows that the classifier trained on the image stimulus data performs just as well on the text stimulus. The average accuracy of the classifier in this case is about 40% (ranging from 26.5 to 56.7%) which is slightly lower than previous conditions.

The confusion matrix for 60% data training and 40% testing is shown in Table 4-2. The presented data in this table is averaged over all 10 subjects. Therefore, it shows the overall confusion between classes. The bold numbers in the main

diagonal show the rate that the true class is correctly predicted by the classifier which is between 30.6 to 37.1%.

Table 4-2 Object imagery classification rate averaged over all subjects

	Classification Result %					
True Class		Cube	Pyramid	Cylinder	Sphere	Cone
	Cube	36.7	16.2	15	18.3	13.7
	Pyramid	16.6	33.6	20.4	13.5	15.9
	Cylinder	16.2	11.5	37.6	15	19.6
	Sphere	16.4	14.6	23.2	30.6	15.3
	Cone	24.1	12.1	8.8	17.9	37.1

Table 4-2 also shows the misclassification rate between any two classes. For example, cube is often misclassified as sphere (18.3%) and pyramid is mostly misclassified as cylinder (20.4%).The misclassification could result from insufficient or inappropriate information in the features. It could also arise from the similarity between certain objects causing the features of different objects to be very close to each other. To test for the latter reason, we determine the number of times a misclassified object occurs as the second choice in a classifier's output.

Table 4-3 shows this result. To read this table, assume that the true class of the object is a "cube". The first row of Table 4-3 shows the number of times the classifier misclassifies the cube as some other object but the true class, viz. cube, is ranked as the second choice. For example, when the classifier for the cube incorrectly classifies the cube as a sphere, 8.3% of the time the cube occurs as the second choice for this classifier. Since the cube classifier classifies a cube as a sphere 18.3% of the time (see the first row of Table 4-2), the proportion of times that the cube occurs as a

second choice when the cube classifier outputs a sphere is 8.3/18.3 = 45.4%. It should be noted that this result is more or less symmetric. In other words, the classifier for the sphere also often confuses the cube with the sphere (see the first column of the fourth row of Table 4-3). A similar confusion can be seen between the cone and the pyramid.

Table 4-3 Classification results of visual object imagery (Top 2 classes) averaged over all subjects in percentage

	Classification Result %						
True Class		Cube	Pyramid	Cylinder	Sphere	Cone	Classification rate (Top 2 classes)
	Cube	-	0.8 (4.9)	0.8(5.3)	8.3(45.4)	0.4(2.9)	46.7
	Pyramid	3.3(19.9)	-	4(19.6)	5.9(43.7)	5.4(34)	52.3
	Cylinder	1.1 (6.8)	1.9(16.5)	-	2.5(16.7)	7.1(36.2)	50.3
	Sphere	6.5(39.6)	5.4(37)	7.1(30.6)	-	3.8 (24.8)	53.3
	Cone	3.8(15.8)	5.4(44.6)	1.1(12.5)	3.6 (20.1)	-	51

One possible explanation is that both the cone and pyramid have angled segments making them different from the other objects. The cube and sphere also have the highest ambiguity possibly because of multiple axes of symmetry. However, it should be noted that this "logical" confusion between similar objects is not entirely consistent. For example, Table 4-3 shows that the cylinder and cone are frequently confused, possibly because of curved segments. Similarly, Table 4-2 shows the cone classifier frequently outputs the cube.

These results points out the possible relationship between the features of the geometry (such as roundedness, sharpness, symmetry and curvature) and the extracted features of EEG signal. For further investigation, we used the classifier

trained on all data of 5 primitive shapes to classify all data of other 15 geometries (S2-set and complex objects). The classification results are shown in Table 4-4.

Table 4-4 Classification result of complex objects with a 5-way classifier for subject

Object ID	1	2	3	4	5	6	7	8	9	10	11	12	13	14	15
Testing set															
	20	0	0	10	10	20	20	20	0	40	0	0	70	20	20
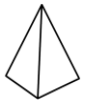	20	40	10	30	30	10	10	10	30	20	30	40	0	10	30
	30	20	30	30	10	10	30	0	10	20	10	40	10	20	40
	10	10	10	10	40	40	10	10	50	0	50	20	10	40	0
	20	30	20	20	10	10	30	60	10	20	10	0	10	0	10

The columns represent the true class while the rows correspond to the classification results for each of the primitive shape classifiers on the complex objects. The underlined numbers in Table 4-4 indicate the most frequent classification output for each training data. As an example, the truncated cone (object 1) is classified most frequently as cylinder (30%). The truncated cone shares more common geometrical features (for example, no sharp edges, round segment) with the cone and cylinder than with other primitive shapes. This may explain why the truncated cone is classified mostly as a cylinder and not a sphere. Also a hexagonal pyramid (object 2) is geometrically more similar to a pyramid (both have angled segments, sharp edges and similar axis of symmetry). This geometrical similarity can be the reason that the hexagonal pyramid is more classified as the triangular pyramid.

However, as the geometrical complexity of the object increases (objects 7-15), there is no strong relationship between geometrical features and the most common classification result. Objects 11 and 13 are two examples of complex objects. Each of these objects is combination of three boxes. The classification outcome shows object 11 is classified as sphere in 50% and never classified as a cube. Object 13, on other hand, is classified 70% as cube and 10% as sphere. It should be noted that we have defined complex objects as a combination of two or more primitive shapes. Therefore, we can divide their geometrical features into two categories. The first category consists of the local features which are related to the primitive shapes forming the complex objects (e.g. roundness of sphere and sharp edges of cube). The second category consists of the global features of the primitive shapes such as

symmetry. In the given example, objects 11 and 13 are created from the same primitive shapes (same local features) but their global features are different. So the output of the classifier may depend on the dominant feature which, in this case, seems to be the global features.

The classification result further indicated that geometrical properties of objects such as roundness and parallel extrusion are also salient in classifying imagined objects which is consistent with Biederman's theory of recognition by components. Biederman [93], [94] proposed that objects are recognized as a combination of primitive objects. These primitives, called geons, can be distinguished from each other by attributes such as curvature, collinearity, symmetry, parallelism and cotermination. Accidental attributes of objects such as color and texture, though cognized, play little part in the recognition.

Therefore, we further examine this hypothesis for mental imagery through two additional binary classifications. Each classifier is designed to distinguish between two opposed geometrical feature (or geons): 1-roundness vs. sharpness 2- parallel extrusion vs. tapered extrusion. All the imagined objects are classified according to these new categories. For example, cube and pyramid are examples of sharpness whereas cylinder and cone are instances of roundness. Two binary classifiers are designed to examine if these features play a significant role in visual imagery. The performance of each classifier is evaluated through a 10 fold validation. In each validation, 50% of data is randomly chosen to train the classifier while the other 50% is used for testing.

The average classification results over all subjects are shown in Figure 4-5. The average classification rate for roundness/sharpness is 69.8% with a standard deviation of 8.2%. Parallel/tapered extrusion classifier has an average accurate rate of 78.2% with a standard deviation of 12.1%. Compared to rate of chance (50%) both of these results are significant with p-value<0.001.

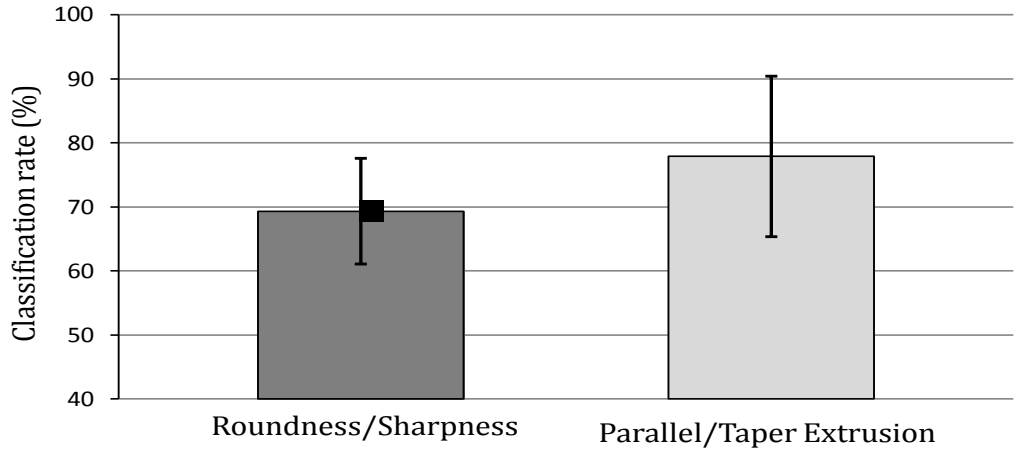

Figure 4-5 Feature Based Classification rate

Most importantly, our analysis of best features in feature-based classifier, revealed that high frequency component (gamma band) in the left frontal cortex has the best predication rate for distinguishing tapered extrusion from parallel.

4.5 Experimental Study 2: Robustness

In the first experiment, the robustness of the classification to the stimulus type was tested by using both image and text cues in two different sessions where the sessions were separated by 20-30 minutes. The classification results show when a classifier is trained with EEG data recorded with image as stimulus, it still can

classify the EEG data associated with another stimulus with an average accuracy of 39.9% (range of 26.5-56.7%). The goal of the second experiment is to evaluate the robustness of classification on EEG data recorded over a longer periods.

For this purpose, we repeated the experimental procedure for sessions 1 and 2 for two subjects over 20 days. We conducted the experiment every other day for twenty days, with two sessions per day and 50 trials per session. There was a 20-30 minute gap between the sessions. This resulted in 100 trials per day per subject. We analyzed the data using two approaches: 1) By classifying the data on a daily basis 2) By training a classifier on the data obtained on the first day and using this classifier to classify the data recorded on the other days. For the first approach, we chose 80% of the data recorded in each day to classify the 20% remaining data of the same day. The top 12 Hilbert spectral features were chosen by using the MWW method. The average classification results of subject 4 over 10 recording days are shown in Table 4-5.

Table 4-5 Classification results of object imaginary recorded over 10 days

		Classification Result %				
True Class		Cube	Pyramid	Cylinder	Sphere	Cone
	Cube	30.4	3.8	18.1	29.4	18.3
	Pyramid	16.8	35.9	14.3	16.1	16.9
	Cylinder	12.3	19.8	39.1	12.9	15.9
	Sphere	32.4	15.1	13.4	28.6	10.5
	Cone	14.8	20.2	16.4	13.2	35.4

The overall classification rate for subject 1 and 2 are 37.5 and 33.9% respectively which is very close to the result of the first experiment shown in Table

(34.9% for subject1 and 34.7% for subject 4). This result shows the repeatability of the procedure when the testing and training data set are recorded in the same day.

To check the robustness of the features over time, we used the data recorded on the first day to train the classifier and then evaluate its performance on the data recorded on the other days. The classification results are shown in Figure 4-6.

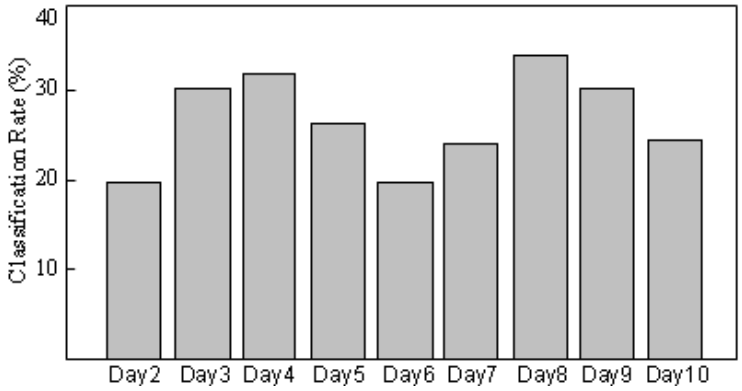

Figure 4-6 Classification rate of data recorded 10 different days when classifier is trained on data of the first day

Based on the result shown in Figure 4-6, when training and testing data are not recorded on the same day, the accuracy of the classifier ranges from 20% (chance) to 35%. This accuracy was previously close to 40% as discussed in section 3.5.

This is mostly due to the non-stationary properties of EEG data which changes the dynamics of the signal over different days. In the analysis process, we normalized the features of each trial with respect to the features of its baseline. This normalization was used to reduce the effect of boredom and fatigue which arise with time in each session. However, to reduce the time effect between different recording days, it seems that further data normalization is necessary.

4.6 Conclusions

This chapter evaluates the feasibility of using the brain computer interface as an interaction device for computer aided design software using visual imagery for geometry representation. Among the six characteristics of visual imagery listed by Cornoldi et al. [86] (specificity, richness of detail, color, saliency, shape and contour & context), all but the shape were fixed. Subjects imagined one of the five primitive objects – a cube, sphere, cylinder, pyramid and cone. The brain activity, collected by the EEG headset, was analyzed using independent components analysis and the Hilbert Huang Transform (HHT). The results show an average classification accuracy of 44.6% over ten subjects (ranging from 36 to 56.4%) in a 5-way classification. Marginal spectra of different frequency bands calculated from Hilbert spectrum of each independent component of EEG data were used as the features of a linear discriminant classifier.

Conducting the same experiment over a longer period (20 days) resulted in an average classification rate of 35.7% over two subjects when the classifiers are trained and tested on a daily basis. Comparing this results to the results of Table 4-2 with the same conditions (4th row), shows the repeatability of the proposed method. However, due to the non-stationary dynamics of the signals, the method does not perform effectively when training and testing data are recorded in different days.

Additionally, the research methodology of using computer images to elicit imagined objects is validated by using text cues as another modality. The fact that classifier can maintain the classification accuracy over different modalities supports the finding of Suppes et al. [95] that show invariance of brain-wave representation of visual image and their name.

This results show that BCIs can be used to distinguish between primitive shapes and thus have the potential for use in CAD systems. However, as the complexity of shape increases, generation and maintenance of visual objects becomes a more difficult task because visual memory cannot hold more than few objects simultaneously [87]. This means that classification of visual imagery may be limited to simple and primitive shapes and may not provide the CAD system the whole capability of object generation. However the classification results of complex objects (Table 4-4) shows a possible correlation between the features of the geometry (such as roundedness, sharpness, symmetry and curvature) and the extracted features of EEG signal. Being able to capture some of the main geometrical features of complex objects will provide the CAD system with some overall information about the object that user intends to create or modify. The correlation between EEG features and geometrical features seems to be very promising for application of BCI in CAD systems and needs further investigation.

It is also important to check the classification result in a real-time system. In the current study, the time required to process and classify an artifact free EEG signal is about 340 ms on a machine with 2.10 GHz AMD Dual-Core CPU. The artifact removal

process used in this study is not real-time. Implementing a real-time artifact removal process will enable the real-time application as a future work.

Another improvement to the techniques described here is the use of other machine learning techniques. In a comparison between linear and nonlinear classifier, Muller et al. [96] showed that kernel-based learning machines such as support vector machine increase the performance of EEG classification. Furthermore, the classification algorithm can be improved by recording data from more locations on the scalp.

However, none of these improvements will make the system totally reliable. Therefore, it might be essential to obtain real-time feedback from the user, possibly through the use of emotional responses of the user. For example, Ko et al. proposed an emotion recognition system based on the EEG relative power value and a Bayesian network [97]. Frustration, meditation, excitement, boredom are some of the emotional states that can be classified [97–99]. In our previous work [100], we have demonstrated that we can detect the satisfaction in human-machine interaction. Detecting the emotional state and user's satisfaction can be used in CAD systems to correct for errors and to strengthen proper classifications. For example, if the BCI system misinterprets a user's imagined object and consequently, the user shows hints of frustration, the BCI can sense this emotion to modify the output till the user's emotional response becomes more neutral. Further experimental studies and software development in this direction is presented in next chapter.

Chapter 5

Satisfaction Detection

This chapter discusses the use of a brain computer interface (BCI) to obtain emotional feedback from a human in response to the performance of machine in an interactive environment. The purpose of this study is to detect the level of human satisfaction and use it as a feedback to correct the machine's misinterpretation of the user's command. This chapter describes experiments and algorithms that use brain activity collected through BCI in order to estimate the level of satisfaction.

5.1 Background on Satisfaction Detection

In human-computer interaction, verbal and non-verbal cues have been widely used to detect human emotion. Vocal tract formation [101], [102], the change in the tone of speech and behavioral speech production process (e.g., duration and pause) are some of the features that have been used to detect the human's emotion from auditory signals [103], [104].

Facial expressions can also be used to detect emotional state. Position or displacement of specific points and regions of the face are used to find a correlation between emotion and facial expression [105], [106]. It should be noted that using facial expression is limited to face-to-face interaction and may not always be detectable. Most recent works interpret anxiety from physiological signals such as heart rate, peripheral temperature, and skin conductivity for emotion detection [107], [108].

However, the main challenge in emotion detection arises from the fact that emotion is an internal state that may not be reflected through behavior. Therefore, facial expression and speech do not always coincide with internal mood. This brings the idea of using EEG signals for detecting the human's emotion. Frontal lobe activity which is characterized in terms of decreased power in certain frequency bands has been consistently found to be associated with emotional states [109]. The best known correlates of emotionality found with EEG involve prefrontal asymmetry-that is, a positive affect is associated with greater activity in the left prefrontal region than in the right side, and negative affect with the reverse [110].

Brain activity signals have been also used to detect the level of emotion during seeing emotionally-charged scenes [111–113]. Zhang and Lee used a combination of functional magnetic resonance imaging (fMRI) and EEG signals to analyze and classify the emotional states stimulated by a natural scene [111]. Schaaff and Schults [112] used single EEG signals recording to classify the human's emotion induced by emotional pictures of three types - pleasant, natural and unpleasant. They reported

an average recognition rate of 47%. Frantzidis et al. [113] used multichannel EEG evoked by pleasant and unpleasant stimuli to classify human's emotion. Using Mahalanobis (MHV) distance-based classifier and support vector machines (SVMs), they could achieve overall classification rates of 79.5% and 81.3% in the discrimination of pleasant and unpleasant emotions.

In this chapter, we investigate the feasibility of EEG based brain computer interfaces for detecting the positive, negative or neutral states of mind of the human in response to a robot's behavior. Section 4.2 discusses the experimental study that we conducted to develop the algorithms. Section 4.3 describes the application of power spectral density, largest Lyapunov exponent and Mann-Whitney-Wilcoxon test to obtain candidate features and to devise classifiers to distinguish between the emotions. Finally section 4.4 presents and discusses the results of the classification.

5.2 Experimental Setup

The goal of this BCI experience is to detect patterns in brain activities and relate them to the mental state (in this case, emotional states). To induce the satisfaction/dissatisfaction, we developed an interactive virtual environment where user is asked to mentally control the motion of a robot through a maze. This is shown in Figure 5-1.

The robots navigation is a combination of three movements: moving forward, turning left and turning right. The experiment involves a human participant who monitors the robots navigation in the maze and tries to correct robots movements.

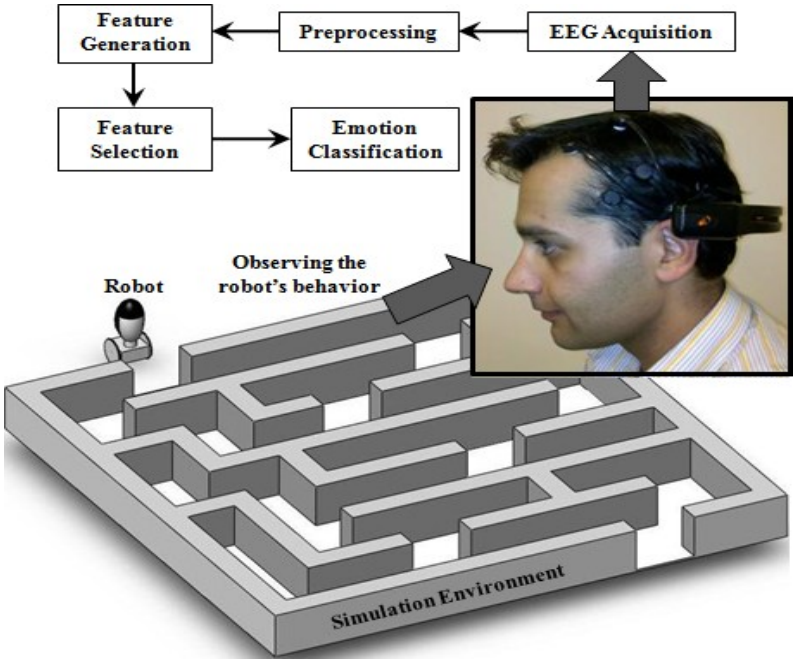

Figure 5-1 Experimental setup for detecting the emotional feedback

Participants were asked to sit in a self-selected comfortable posture, 40 cm away from a computer screen. They were then asked to mentally control the navigation of the robot through the maze in the simulation environment.

The robot navigates in the maze through a sequence of movements. Each movement consists of two parts. During the first part (mental command), the direction that the robot should go is shown to the participant visually on the computer screen.

The participant is asked to mentally control the robot's motion on the screen in that given direction. For example, an image of a right arrow appears on the screen to indicate that the user is to imagine the robot turning to the right. Mental command lasts for about 2 seconds and the robot does not move during this time. During mental command, the participant will be in a neutral state of emotional arousal.

The second part of the movement is the response of the robot to the mental command. In reality, the participant does not have control over the robots motion. The sequence of turns has been predetermined and occurs regardless of the users control input. Thus, sometimes the robot turns in the direction desired by the user and sometimes it turns in the opposite direction. Correspondingly, the participant will experience satisfaction in the former cases and dissatisfaction in the latter cases.

EEG data is recorded continuously during each part of the movement. EEG data during mental command is labeled as "Neutral". If the direction of mental command and robots respond are the same, we label the EEG data recorded during the robot response as "Satisfied" otherwise it would be labeled as "Unsatisfied".

We conducted this experiment with four male subjects (aged between 21 and 35) in two different sessions. Each session requires 74 movements (148 data point) for the robot to complete the maze. It thus gives a total number of 1184 data points. 80% of these are used for training the classifiers and the remainder is used for testing. Before extracting the features, the first and the last 10% of the recorded trial for each movement are chopped to eliminate the transitional effects.

Figure 5-2 shows the signal at channel F3 for two movements. Each movement has two data segments. In the first movement, the direction of robot's movement is the same as mental task and therefore the data segment associated with 1st robot response is labeled as "Satisfied". However in this second movement, the two

directions are not the same and data segment is labeled as “Unsatisfied”. All data segments associated with mental command are labeled as neutral class.

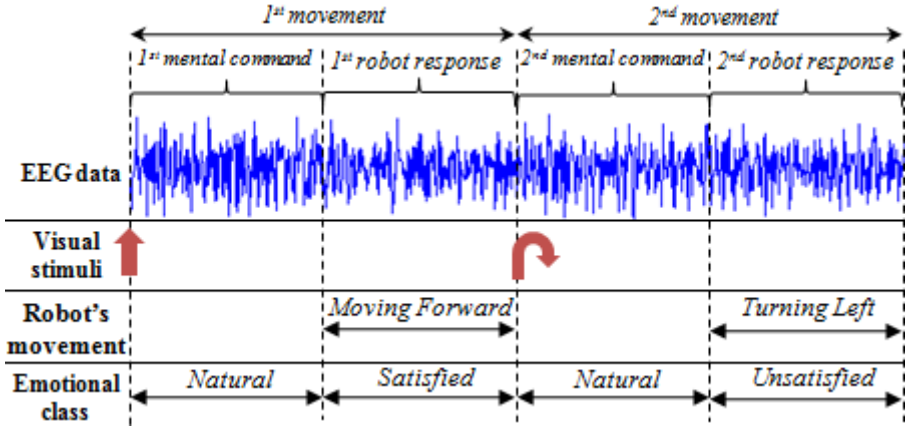

Figure 5-2 EEG data recording during two mental tasks and their associated labels

5.3 EEG Analysis

To analyze the EEG signals, five frequency bands are usually considered: delta (0-4Hz), theta (4-8 Hz), alpha (8-13 Hz), beta (13-30 Hz) and gamma (30-100 Hz). It has been shown that the power of these sub-bands carry useful information about the emotional states [114], [115]. Davidson et al. [114] have shown that disgust caused less alpha power in the right frontal region than happiness while happiness caused less alpha power in the left frontal region. Moreover, Kostyunina and Kulikov [115] found that that the peak in the alpha frequencies increases when the participant experiences joy or anger, and decreases when the participant feels fear or sorrow. Both spatial and temporal features of EEG sub-bands have been used in BCI applications. Some of these features are: amplitude value of EEG signals, [114] power spectral density (PSD) values [97], [116] and higher-order crossings [98].

It has been shown that EEG signals exhibits complex behavior with nonlinear dynamic properties [117]. This behavior takes the form of EEG patterns with different complexities. Considering this, nonlinear dynamics theory may be a better approach than traditional linear methods in characterizing the intrinsic nature of EEG. Some researchers have used nonlinear based features of EEG signals such as largest Lyapunov exponent and fractal dimension [118], [119].

In this chapter, we use a combination of power spectral density (PSD) of different EEG sub-bands and the largest Lyapunov exponent (LLE) of EEG signals at each electrode location as our set of features.

5.3.1 Power Spectral Density

To estimate the power spectrum of EEG signals, we implemented the Welch periodogram algorithm-one of the most commonly used techniques to compute the power spectrum. EEG signals for each mental task were divided into segments of one second, with a Hanning window of the same length applied to each segment, and 50% overlapping between the segments. This provides us with a frequency resolution of 1 Hz. Five frequency band powers from the delta, theta, alpha, beta and gamma bands were extracted. For each data point, normalized power spectral density of sub-band '*b*' at electrode location `*l*' (PSD_{bl}) is calculated as following:

$$\overline{PSD_{bl}} = \frac{PSD_{bl}}{\sum_{b=1}^{5} PSD_{bl}} \tag{5-1}$$

This produce 5 features at each electrode location which makes a total number of 70 features for each data point.

5.3.2 Lyapunov Largest Exponent

The Lyapunov Exponent (λ) measures the sensitivity of a dynamical system to initial conditions. For a dynamical system in an m-dimensional phase space, there exist `m' Lyapunov exponents (spectrum of Lyapunov exponents). Each Lyapunov exponent (λ_i) defines the exponential average rate of divergence of two neighboring trajectories in one direction of the state space. A positive Lyapunov exponent corresponds to divergence of trajectories (existence of a chaotic attractor). A negative exponent implies the convergence of trajectories to a common fixed point. Finally, a zero exponent means the trajectories maintain their relative positions (they are on a stable attractor-limit cycle).

To construct m-dimensional phase space from EEG time series signal, we used the reconstruction technique developed by Packard et al. [120]. For a given EEG signal, $x(t)$, m-dimensional phase space is formed by using delay coordinate,'τ' as shown in Equation 5-2.

$$X_i(t) = [x(t_i), x(t_i + \tau), ..., x(t_i + (m-1)\tau)] \quad i = 1,2,...,m \tag{5-2}$$

The algorithm proposed by Wolf et al. [121] is used to compute the Largest Lyapunov Exponent (LLE) from each EEG data. We locate nearest neighbor to initial point as Equation 5-3.

$$X_i(t_0) = x(t_0),\ x(t_0 + \tau), ..., x(t_0 + (m-1)\tau) \tag{5-3}$$

Then the Lyapunov exponent can be defined by Equation 5-4.

$$\lambda_i = \frac{1}{t_m - t_0} \sum_{k=1}^{m} \ln \frac{L(t_k)}{L(t_{k-1})} \tag{5-4}$$

Where $L(t_0)$ is the initial distance between these two nearby trajectories and $L(t_k)$ is a distance between them at a later time t_k.

To implement this algorithm, OpenTSTOOL developed by Merkwirth et al. [122] is used. In our analysis, we use an embedding dimension of m=8 and delay of 10 sampling time as they show the best results. Therefore, there are eight Lyapunov exponent associated with each EEG data from which we select the four largest one as the features of each EEG signal. This will form a total number of 56 LLE features per sampling data.

5.3.3 Feature Selection

In dealing with EEG classification, an important problem is the huge number of features. This arises because (i) EEG signals are nonstationary, thus features must be computed in a time-varying manner and (ii) the number of EEG channels is large (14 channels which produce total number 126 features).

To evaluate which of the features provides the most useful information about the emotion, we used Mann-Whitney-Wilcoxon (MWW) test. The MWW test is a non-parametric test for determining whether two independent samples of observations belong to the same distribution. We rank all the features by Mann-Whitney-Wilcoxon (MWW) test in three binary classifications (each class vs. the other two classes). Therefore, we get three rankings for features that each represent the most important features of its corresponding class. The features that have the highest rank in all three tests are selected as the final feature set for the classification.

To get more insight into the information carried by each features, we also ranked all the features based on the electrode location. Figure 5-3 shows the classification rate of each of three classes just by using all features of single electrode. This figure suggests that using feature of channels AF3, T7 and P8, almost the maximum classification rate for all three emotional states is achievable.

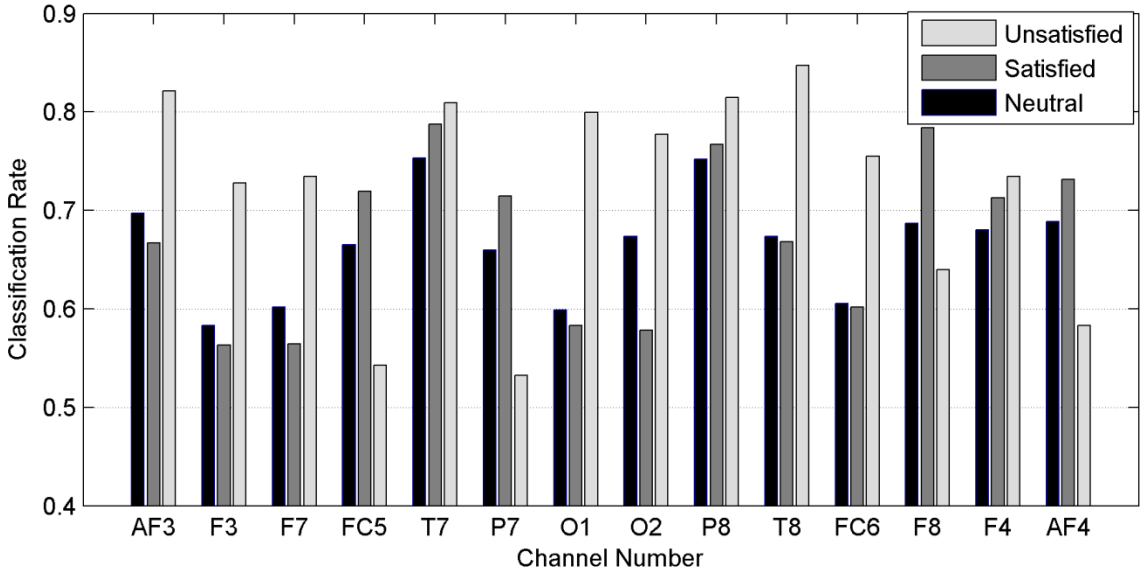

Figure 5-3 Classification rate of different channels features

The extracted features of these channels and their symmetric locations are used in a multi-class LDA classifier as the primary classification. The results and final classifiers are presented in next section.

5.4 Results and Discussions

We used 80 % of the recorded data for training the classifier with three classes of “neutral”, “satisfied” and “unsatisfied”. To compare the effect of the types of features on the classification rate, we used three sets of features to train the

classifier. Table 5-1 to Table 5-3 show the results of classification for each of the classifier (when only LLE, only PSD and finally, both the LLE and the PSD are used).

Table 5-1 Classification result with just using LLE

Class	Neutral (True)	Satisfied (True)	Unsatisfied(True)
Neutral (output)	71.6	15.3	13.1
Satisfied (output)	16.9	78.3	4.8
Unsatisfied (output)	11.5	6.4	82.1

Table 5-2 Classification result with just using PSD

Class	Neutral (True)	Satisfied (True)	Unsatisfied(True)
Neutral (output)	68.1	20.6	11.3
Satisfied (output)	18.1	77.4	4.5
Unsatisfied (output)	13.8	2.0	84.2

Table 5-3 Classification result with both using LLE and PSD

Class	Neutral (True)	Satisfied (True)	Unsatisfied(True)
Neutral (output)	63.1	22.1	14.8
Satisfied (output)	14.4	73.1	12.5
Unsatisfied (output)	22.5	4.8	72.7

The results show that the rate of detecting “unsatisfied emotion” is significantly larger than neutral and satisfied emotions. There is no surprise to see that most of misclassification involves “neutral emotion" which is a margin between the other two classes.

We compared the classification rate of the three mentioned conditions with the number of features. Furthermore, we used a fourth method where each EEG data is

classified three times (each time with one of the feature sets mentioned above). The results of these classifiers are diffused using a voting scheme shown in Figure 5-4.

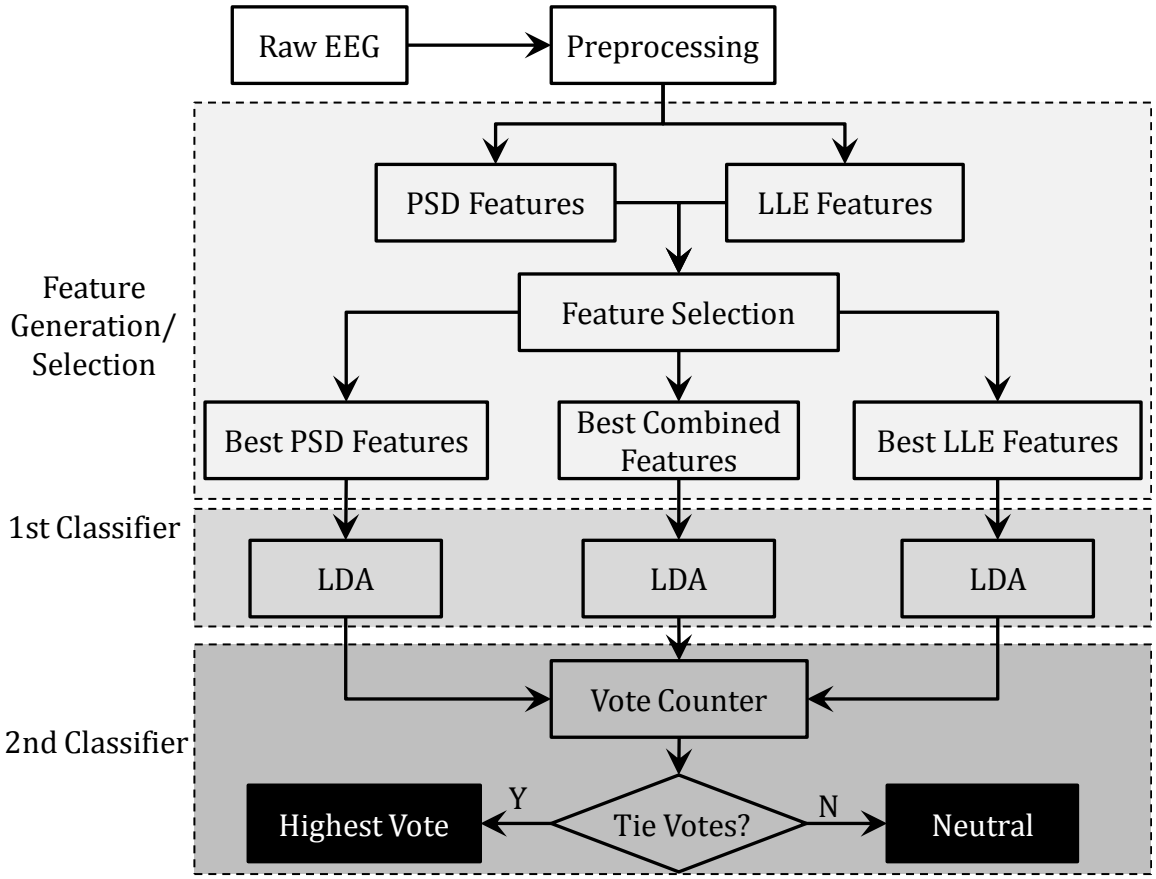

Figure 5-4 The algorithm for calculating the final classification result.

In the voting classifier, if at least two of the classifiers determine that a data segment belongs to the same class, the classification result will be this class. Otherwise, when none of the classifiers have the same outcome, the data will be classified as neutral.

Figure 5-5 illustrates the classification rate versus the number of feature when different types or combination of features are used. Figure 5-5 shows that combining both features does not significantly change the classification result.

However, using all the features, according to the voting technique (Figure 5-4), increases the accuracy of the classifier up to 80%.

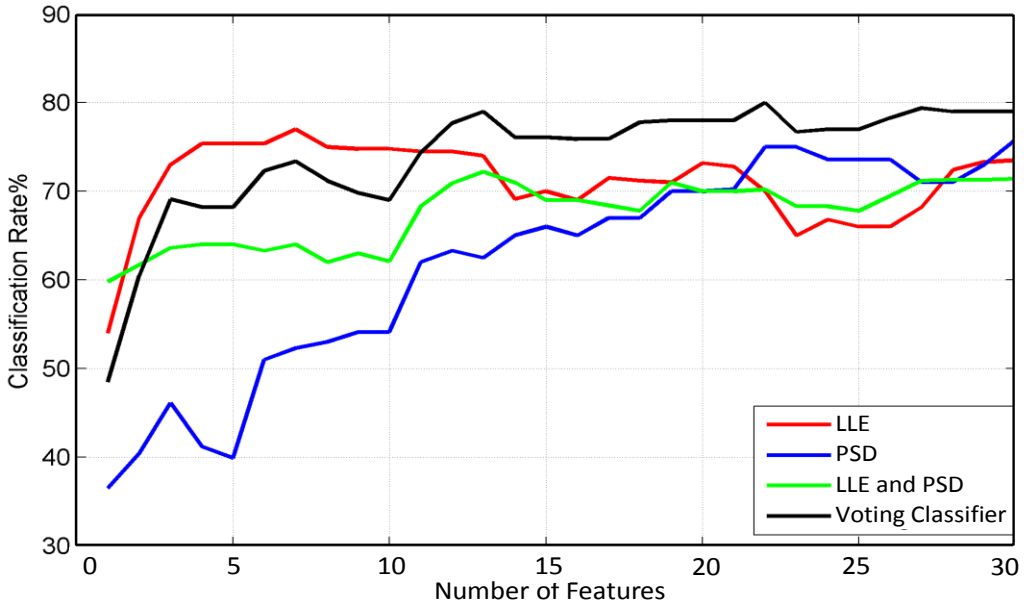

Figure 5-5 Comparison of classification rate of type and number of features.

Comparing the four different types of features in Figure 5-5, it appears that when the highest accuracy with the minimum number of features is obtained using the LLE. . The LLE can achieve a classification accuracy of 75% using 4 features. Just using PSD features, we need a larger size of feature vector to get to the same classification rate. However, increasing the size of feature vector in LLE will result in a less accurate classifier. This suggests that there are only a few electrodes or sub-bands carrying suitable information about the emotional state in form of LLE. The information is more spread out for the PSD.

Classification rate based on channel information for both LLE and PSD features is shown in Figure 5-6 and it appears that PSD features of T8 and P8 channels improve the accuracy the most.

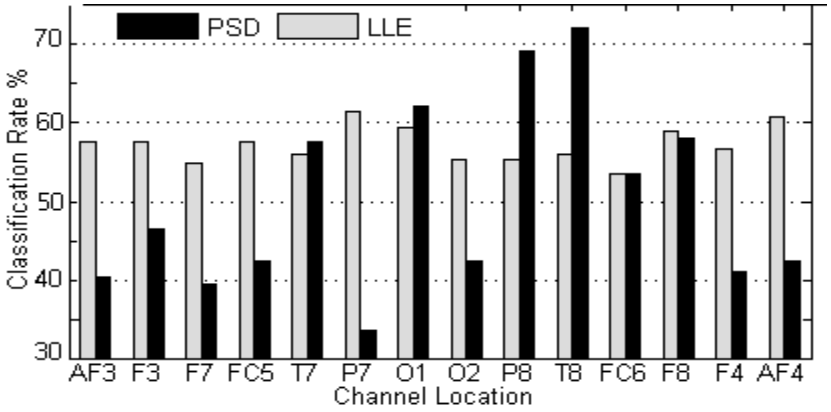

Figure 5-6 Comparison of classification rate of type and location of features.

Subject based classification results for the four feature types are shown in Figure 5-7. As illustrated in Figure 5-7, using the voting method between three LDA classifiers gives the highest accuracy level for the subject based classifier. These classification rates vary between 80-95% for different subjects.

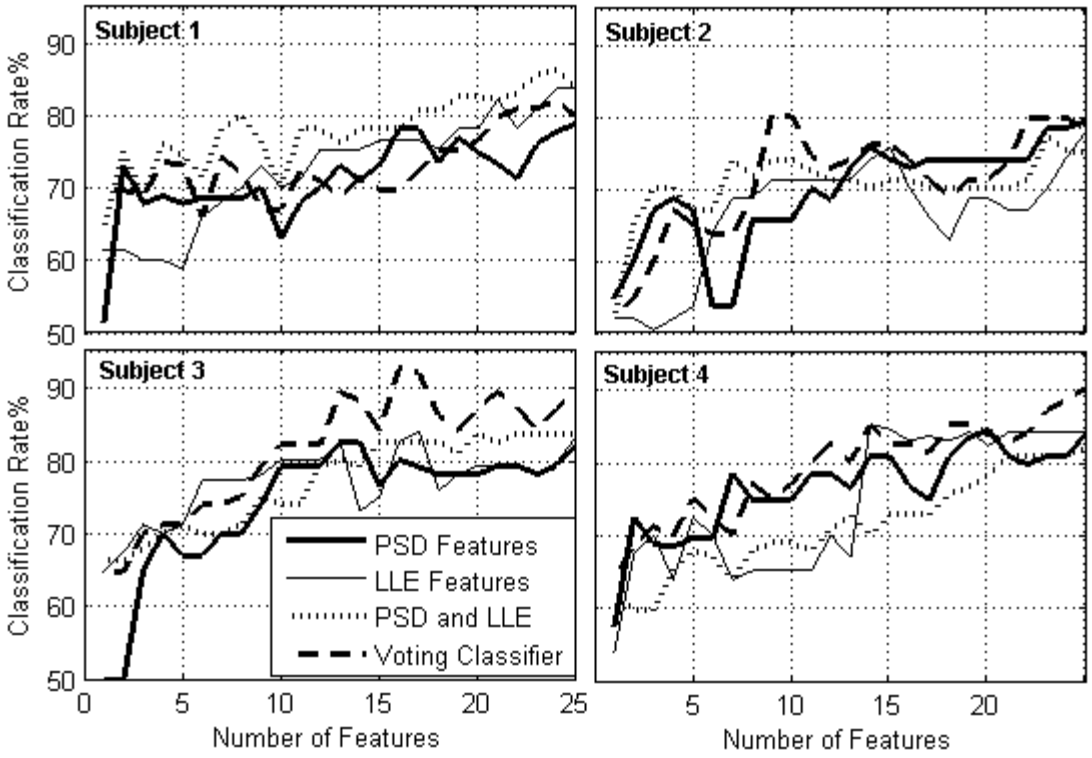

Figure 5-7 Subject based classification for emotion detection

The fact that the accuracy of overall classification is less than the subject based may be because the emotional response of different participants to the same event is not the same.

5.5 Summary

In this chapter, we used an EEG-based brain computer interface to detect the satisfaction of human in response to performance of a machine in an interactive environment. By conducting an experience with a simulated robot that does not always follow the human desires, we collected a series of brain activity data using the electroencephalogram (EEG). We then used the power spectral density and Lyapunov largest exponent to construct 112 features.

Ranking the feature with Mann-Whitney-Wilcoxon test, the top ranked members of each feature set were selected for classification purposes. Comparing different type and combination of features, the best classification rate (79.2%) is achievable by considering the results of three single classifiers. Furthermore, the accuracy of subject based emotional classification can be much higher than the overall accuracy with using the same method (80.2%-94.7%). However, using a subject based classifier needs new training data for each subject. For future work, an adaptive classification method seems to be a wise choice as it can pre-trained based on emotional response of a large group of subjects and then adapted as it interacts with a new user.

Chapter 6

Object Modification

This chapter describes experiments and algorithms that use the BCI for selecting and modifying geometrical objects. The first part of the chapter discusses a method to select different surfaces of geometrical objects in the CAD systems using the P300 wave. The P300 (P3) wave is an event related potential (ERP) elicited by infrequent stimuli (target faces flashing). Users wear an electroencephalogram (EEG) headset and try to select a target face of an object. Different faces of the object randomly flash. Since there are several faces, the target faces flashes relatively infrequently compared to the non-target faces. This makes the flashing of target face an infrequent event. The EEG data is analyzed with a combination of morphological features and discrete wavelet transforms (DWT) to detect the P300 component in the signal. The flashing face which causes the P300 component in the EEG signal is classified as the target face. Using linear discriminant analysis, the target face is classified correctly with an average accuracy of 78.7%.

In the second part of this chapter, the selected surface is modified by employing the state-of-the-art in motor imagery. In such applications, it is important to detect when the user is interested in moving an object and when the user is not active in this task. The second part of this chapter evaluates the steady state visual evoked potential (SSVEP) as a feedback mechanism to confirm the mental state of the user during motor imagery. These potentials are evoked when a subject looks at flashing objects of interest. Four different experiments are conducted in this chapter. Subjects are asked to imagine the movement of flashing object in a given direction. If the subject is involved in this task, the SSVEP signal will be detectable in the visual cortex and therefore the motor imagery task is confirmed. During the experiment, EEG signal is recorded at four locations near visual cortex. Using a weighting scheme, the best combination of the recorded signal is selected to evaluate the presence of flashing frequency. The experimental result shows that the SSVEP can be detected even in complex motor imagery of flickering objects. The detection rate of 85% is achieved while the refreshing time for SSVEP feedback is set to 0.5 seconds.

6.1 Surface Selection: P300 Approach

The event related potential (ERP) is one of the main methods in using EEG-based BCI. ERPs are electrophysiological responses of the brain to an internal or external stimulus. The most robust feature of the ERP is a positive peak that occurs around 300ms after stimulus. This positive peak is known as P300 or P3 [123].

The ERP waveform consists of a sequence of positive and negative peaks in the recorded data [51] labeled as P1, N1, P2, N2, and P3 (also known as P300) as shown in Figure 6-1. The initial peak (P1) is an obligatory sensory response that is elicited by visual stimuli without cognitive processes. The P1 wave is strongly influenced by stimulus parameters such as luminance. The early sensory responses are called exogenous components to indicate their dependence on external rather than internal factors. By contrast, the P300 wave depends entirely on the task performed by the subject and is not directly influenced by the physical properties of the eliciting stimulus. The P300 wave is therefore termed an endogenous component to indicate its dependence on internal rather than external factors.

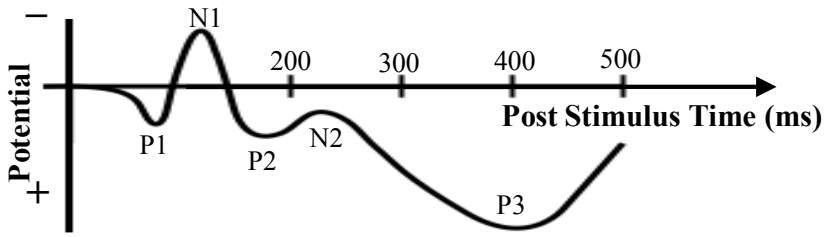

Figure 6-1 main ERP components: P1, N1, P2, N2, and P3

P300 as a main component of the ERP is considered a potential signal for detection and implementation in BCI. P300 is a positive EEG deflection that occurs during 200–700ms (typically 300 ms) after stimulus onset, and is typically recorded over the central-parietal scalp [12]. The response is evoked by attention to rare stimuli in a random series of stimulus events (i.e., the oddball paradigm).

Farwell and Donchin (1988) were the first to develop a P300 based BCI [51]. They introduced the P300 speller system, which enabled subjects to spell words by

sequentially choosing letters from the alphabet. All alphabets were placed in a 6x6 matrix whose rows and columns were randomly flashed. P300 component would be detected after the flash of the row or the column on which the target letter was.

Since the work of Farwell and Donchin, most of the research on P300 based BCIs were focused either on developing new algorithm for P300 detection or on creating new application scenarios to use P300 component [50], [124].

Hoffmann et al. presented a six-choice P300 paradigm which was successfully tested on five disabled and four non-disabled subjects. They used six different images (each representing a specific action) which were flashed in random order with a stimulus interval of 400 ms [124]. More recently, Campbell et al., demonstrated a brain-controlled address book dialing application for cell phones which works on similar principles to P300-speller [125].

As it is illustrated in Figure 6-2, the similarity of all these applications is to place all possible choices in a static grid. Different rows and columns of the grid flash randomly while the algorithm detects the P300 components.

Figure 6-2 Different BCI application based on P300 (a) P300 speller [51] (b) Smart home [124] (c) smart phone address book [125]

6.1.1 Experimental Method

The experiments for selecting surfaces of a CAD model are conducted as a series of trials. In each trial, a target surface of an object is shown to the subject. The subject is then is asked to focus on the target face as the experiment starts and count silently how often the target face is flashed. The experiment begins with flashing two random faces of the object for about 100 ms. Post stimulus EEG signals are record for 750 ms. Then two other faces flash (2nd stimulus). The sequence of flashes is block-randomized. This means that if the object has n faces, after n/2 flashes, each face is flashed once, after n flashes each face is flashed twice, and so on. The number of blocks is chosen randomly between 8 and 10. Therefore each face flashes 16 to 20 times in each run. Figure 6-3 shows the time course of an experiment.

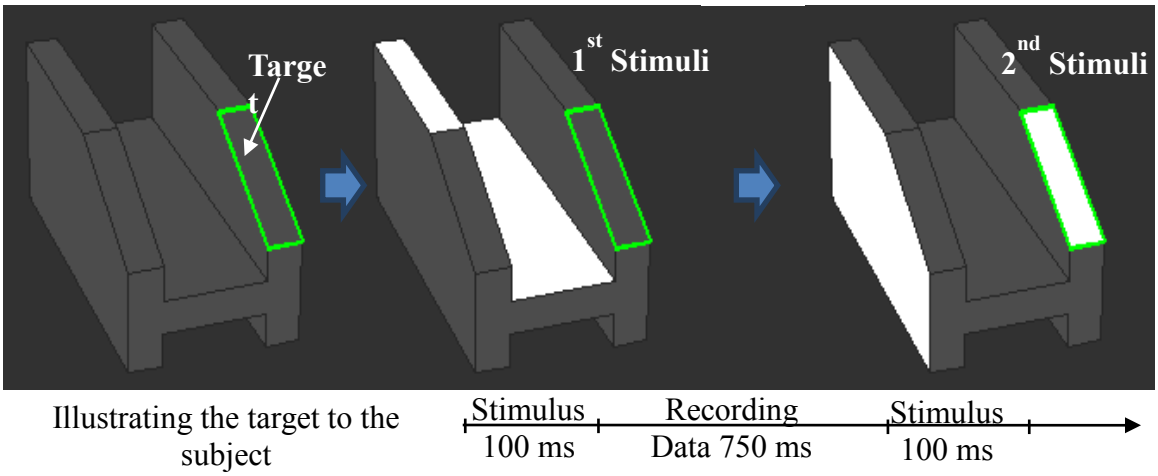

Figure 6-3 Time course of the P300 experiment for face selection

The experimental study consists of 4 subjects and each subject participated in four sessions at two different days (two sessions per day). The 3D object, shown in Figure 6-3, was used as a target object. Each session consists of 8 runs per subject (one run per each face). This gives 32 runs per subject. On the verge, each face flashes 18 times in each run. Thus, a total number of 144 trials per face in each run is recorded of which 126 (18*7) are non-target (Non-P300) and 18 are target faces (P300).

After removing the artifacts, a 6th order forward-backward Butterworth band pass filter with cut-off frequencies of 1.0 Hz and 30 Hz were used to filter the data.

6.1.2 Discrete Wavelet Transform

The Discrete Wavelet Transform (DWT) is a time-scale transformation which provides both temporal and spatial information about a signal. The DWT of a time series signal *X(t)* is defined by Equation 6-1.

$$W(j,b) = \sum_{j}\sum_{b} \frac{1}{\sqrt{2^{j}}} X(t)\psi\left(\frac{t-b}{2^{j}}\right) \qquad (6\text{-}1)$$

Where in Equation 6-1, $\psi(t)$ is a time function with finite energy and fast decay called which is known as mother wavelet. Wavelets, $\psi_{a,b}$, are the orthogonal functions which are obtained from the mother wavelet through dilation and shifting process which is shown in Equation 6-2.

$$\psi_{a,b}(t) = \frac{1}{\sqrt{a}}\psi\left(\frac{t-b}{a}\right) \tag{6-2}$$

Where in Equation 6-2, a is the dilation coefficient and b is the time shift. In the wavelet space, the time series $X(t)$ can be represented as an inner product of wavelets and its coefficients as shown in Equation 6-3.

$$X(t) = \sum_{j,b} d_j(b)\psi_{a,b} \tag{6-3}$$

Where $d_j(b)$ denotes the wavelet coefficients at scale *j*. An efficient way to calculate the coefficients at different levels is using multi-rate filter bank [126]. Ths original signal *X(t)* will pass through a successive high-pass and low-pass filtering The dilation coefficient ($a = 2^j$), down sample each sub-band by two so that it contains half the samples of the neighboring higher frequency sub-band. This process is shown in Equations (6-4) and (6-5):

$$a_j(k) = \sum_m \bar{h}(m-2k)\, a_{j+1}(m) \tag{6-4}$$

$$d_j(k) = \sum_m \bar{g}(m-2k)\, a_{j+1}(m) \tag{6-5}$$

Figure 6-4 shows a two-level filter bank which decompose the original signals into low-pass coefficients, $a_j(k)$, and high-pass coefficient $d_j(k)$ which are also

known as approximation and detail coefficients, respectively. This process can be iterated to decompose a signal up to any desired resolution level.

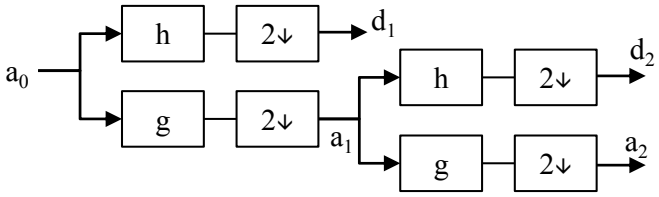

Figure 6-4 Two level wavelet filter bank if the sub-band coding algorithm

Quadratic B-Spline functions are shown to have similarity with evoked response and therefore, are used as mother wavelets in this study [127].

The EEG signal is recorded at sampling frequency of 128 Hz and therefore by decomposing the signal into four octaves, five set of coefficients are obtained which are associated with the following frequency bands:

d1: 32-64 Hz d2: 16-32 Hz d3: 8-16 Hz d4: 4-8 Hz a4: 0-4 Hz

Prior to DWT, the frequency components of the signal which were above 30Hz were filtered. Therefore d1 coefficient does not contain useful information. The rest of coefficients represent the signal information in the following frequency bands:

a4: Delta band: 0.3–4 Hz, d4: Theta band: 4–8 Hz

d3: Alpha and lower Beta: 8–16 Hz d2: Higher Beta band: 16–30 Hz.

We use 8 coefficients of the delta and theta band, 8 wavelet coefficients of alpha and lower beta band and 16 coefficients of the higher beta band of the post-stimulus epoch. This yields a total number of 32 wavelet features per channel. Since the P300 is more observable at peripheral cortex, we average the signals at symmetric

locations (e.g O1 and O2, P7 and P8) and extract the features from 7 average artifact free signals.

In addition to wavelet features, we use a set of morphological features proposed by Abootalebi et al [128]. The morphological features are calculated in time domain and are listed as following:

1- Latency (LAT): the time between 200 and 750 post stimulus where the signal is maximum

2- Amplitude of the maximum signal

3- Latency-Amplitude ratio

4- Positive area under the curve

5- Negative area under the curve

6- Average absolute signal slope

7- Peak-to-peak value

8- Peak-to-peak slope

9- Number of zero crossing

Therefore we extract a total number of 224 wavelet and 63 morphological features for each EPOC in each trial.

6.1.3 Classification

Since we are dealing with a binary classification for each signal (target vs. non-target), we rank the key features by a class separability criteria. We use Bhattacharyya distance as the measure for separability of binary classification. This distance measures the similarity of two discrete or continuous probability distributions by measuring the amount of overlap between the two populations. Therefore the highest ranked set of features by this criterion projects the sampling data of two classes into two spaces that have the minimum overlap (or maximum distance) with each other. Using this criterion, we select the top 10 features for the

classification purpose. Finally, the selected features are classified by a linear discriminant analysis (LDA).

6.1.4 Results and Discussion

The main aim of the LDA classifier is to check if the recorded EEG signal contains the P300 component. However, the ultimate goal of the experiment is to detect the face of the cube that subject was trying to select. The P300 component is seen in signal associated with a rare event. Therefore, the more the stimuli are presented (more the number of flashing), the higher the probability of detecting the P300. Based on this fact, 4 trials of each run in each session (16 trials) are randomly selected to calculate the ERP of each face for training. Therefore the remaining 14 trials in each run can be used to calculate the ERP of the corresponding face for testing. Each ERP is classified as P300 or nonP300 component. If the classifier detects P300 component in ERP of more than one face, it will be considered as an ambiguity and counted as failure in calculating the classification rate. This whole evaluation is repeated five times, where the training data is randomly selected in each time.

The classification method is subject based. Each subject performs 8 runs in each of the four sessions. This means that the performance of each subject is evaluated through 32 target face and 224 non-target faces. The classification results are presented in Table 6-1. The numbers in the parenthesis show the standard deviation of classification rate in 5 evaluations.

Table 6-1 Classification Result in 5 random evaluations averaged over all subjects

Subject	Correct Target Detection	Incorrect Target Detection	Ambiguity in classification
Sub. 1	80.62 (± 3.75)%	10.62 (± 5.0)%	8.75 (± 3.75)%
Sub. 2	80.00 (± 4.37)%	10.62 (± 8.12)%	9.37 (± 3.12)%
Sub. 3	76. 25 (± 8.12)%	11.87 (± 6.87)%	11.87 (± 13.12)%
Sub. 4	78.12 (± 9.37)%	12.5 (± 6.25)%	9.37 (± 12. 5)%

The presented classification results in Table 6-1 show that overall performance of the proposed algorithm is 78.7%. It can also be seen that the ambiguity rate in considerably larger than misclassification. Ambiguity in the classification means that in addition to true target face, P300 component has been detected in another face too.

For each face, we only consider six out of eight runs for P300 detection. So it is possible that P300 component may not be detectable in all trials of the true target face. This condition can be followed by a misclassification in P300 detection of a non-target face. Together these two conditions will cause confusion in detecting the true target face. By increasing the number of flashes in each trial this issue can be addressed. However increasing the number of flashes will cause a longer wait for user to select a target face which is subjected to fatigue in long term application.

The effect of number of trials in classification performance is studied by changing the number of trials in ERP from 8 trials to 14 trials. The results are evaluated through 5 classifications.

Figure 6-5 illustrates the results for all four subjects. It can clearly be seen that using a lower number of trials for classification will result in lower classification

accuracy. As the number of trials decreased, the signal to noise ratio will be decreased too, which makes the P300 detection more difficult.

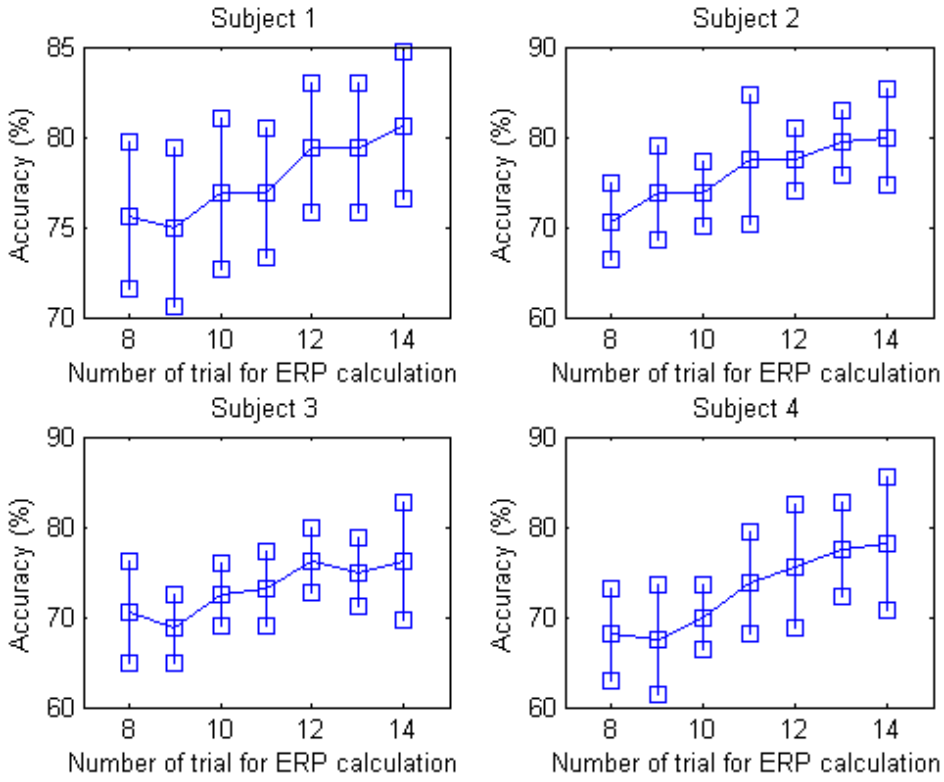

Figure 6-5 The effect of number of trials in ERP on classification results

Another source of ambiguity and misclassification is the method used for stimulus presentation. The main idea behind P300 detection is to make the event that is desired for the subject a rare event. This is achievable through having some non-ideal events repeated more frequently. For this reason, all the faces of an object regardless of their size and location are randomly flashed.

During the stimuli presentation it may often occur that the target face is surrounded with relatively larger faces with which it may overlap. Therefore when such a face is flashing it may cause a visual error in the subject and make either

flashing a non-target face as a rare event or make the flashing of the target event as frequent as the other events.

6.2 SSVEP Feedback for Motor Imagery Engagement

Motor imagery i.e. the imagery involved in motion has been the primary focus of most BCIs. Here signals are obtained during imagined sensorimotor rhythms (SMR). Typically, the SMRs are detected based on features of the μ and β rhythms (8–12 and 18–26Hz) [129]. Changes in the amplitudes of these frequency bands are referred to as event-related desynchronization (ERD) (i.e. decrease) and event-related synchronization (ERS) (i.e. increase). The rhythms decrease or desynchronize with movement or its preparation, and increase or synchronize after movement and with relaxation [130].

BCIs based on sensorimotor rhythms (SMR) are the basic elements for movement control in virtual environments. It has been shown that using SMR based BCI, it is possible to control the 2D motion of a cursor [78], [131].

The main advantage of motor imagery classification is that it requires no external stimuli and the ongoing EEG is used to classify the mental task. However, its implementation in continuous human computer interaction is subjected to false detection of movement because certain brain activities involved even in an idle state can mimic motor imagery. Despite all the research and improvement in BCI system, there are still about 20% of subjects who are not able to use BCI with effective performance [132]. Therefore in order to use BCI as an alternative in human

computer interactions, it is critical to increase its robustness. To overcome these problems, we propose a hybrid BCI approach. This approach uses a stimulus based response such as P300 or visual evoked potential in conjunction with sensorimotor rhythms to increase the robustness of the BCI [132], [133].

Similarly, to reduce the false alarm in classification of ongoing EEG signals, Pfurtscheller et al [134] have proposed a brain switch by combining visual evoked potential and event related synchronization (ERS)-based BCI. Although they could achieve high robustness by combining SSVEP and ERS, their hybrid BCI is only designed to detect one mental task and may not have the same performance in complex situations.

In this chapter, we have conducted a series of experiments to verify the robustness of hybrid BCIs in multi-mental task situations. To this end, steady state visual evoked potential (SSVEP) is used in combination with different motor imagery. The basic idea is as follows: in human computer interaction, motor imagery usually occurs when the subject is gazing on a virtual object to move or rotate. Therefore by flashing the object of interest on the screen, it may be possible to get passive confirmation about correct detection of user's intent. This passive confirmation (feedback) is achieved through SSVEP detection.

6.2.1 Steady state visual evoked potential

Among different brain signals that have been employed for EEG based BCIs, VEP (Visual Evoked Potentials) based systems have been studied since 1970s [135]. It is commonly accepted as a method that provides high information transfer rate and

needs less user training. VEP is the response of human brain to the visual stimulus. It is categorized into transient VEP (TVEP) and steady state VEP (SSVEP). These correspond to visual stimulus with low and high frequency, respectively. TVEP arises when the stimulation frequency is less than 2 Hz, while SSVEP appears when the repetition rate of the stimulus is higher than 6 Hz [52].

It is well agreed that SSVEP has a wider area of application than TVEP because in most cases, the human's brain is considered in steady state of excitability in which the responses that elicited by the high frequency visual stimulus will overlap each other. Since the characteristics caused by two kinds of stimulus are different, researchers usually use temporal methods for TVEP analysis and frequency analysis for SSVEP case [136].

A Steady-State Visual Evoked Potential (SSVEP) is a resonance phenomenon arising mainly in the visual cortex when a person is focusing his/her visual attention on a light source flickering with a frequency above 6 Hz [52].

The SSVEP can be elicited up to at least 90 Hz [137] and could be classified into three ranges: low (up to 12 Hz), medium (12-30) and high frequency (> 30 Hz). In general, the SSVEP in low frequency range has larger amplitude responses than in the medium range. Thus, the lower frequencies are easier to detect.

The high-frequency SSVEP ranges have the advantage of a minimum visual fatigue caused by flickering, making the SSVEP-based BCI a more comfortable and stable system [138]. At a same time, these frequencies experience the weakest

SSVEP which make the SSVEP detection a more difficult task and requires computationally expensive algorithms.

6.2.2 SSVEP Experiments

EEG signals were recorded using the Emotiv neuroheadset at 4 channels on the scalp. The names of channels that are used for this study are based on the international 10-20 system are: P7, O1, O2, and P8. Signals were recorded at sampling rate of 2048 Hz, and sent to the computer wirelessly after being down-sampled to 128 Hz.

The selected visual stimulation was a three-dimensional cube that flashed on the screen. The background is black while the cube had white surfaces and blue edges. All surfaces of the cube were flashing at a frequency of 13 Hz.

Four different experiments were conducted in this study. Each experiment consists of two parts: part one is conducted in only one trial during which the cube is not flashing. In this part of the experiment, subject is asked to gaze at the object and conduct an imagined movement in a given direction. This experiment only contains motor imagery and therefore can be used as the control. Part two contains 5 trials in which the subject is performing the same task as part one but with presence of the flashing stimulus. In each trial for all experiments, the subject is asked to sit on a comfortable position and look at the screen. EEG data for each trial is recorded once the cube appears on the screen until it disappears.

The motor imagery task that subject is instructed to perform each experiment are shown in the Figure 6-6. The arrows indicate the cube's motion (rotation vs.

translation) and its direction. The numbers denote different states during the experiment. The arrows and numbers in the figures are only for the convenience of description and do not exist in the experiment.

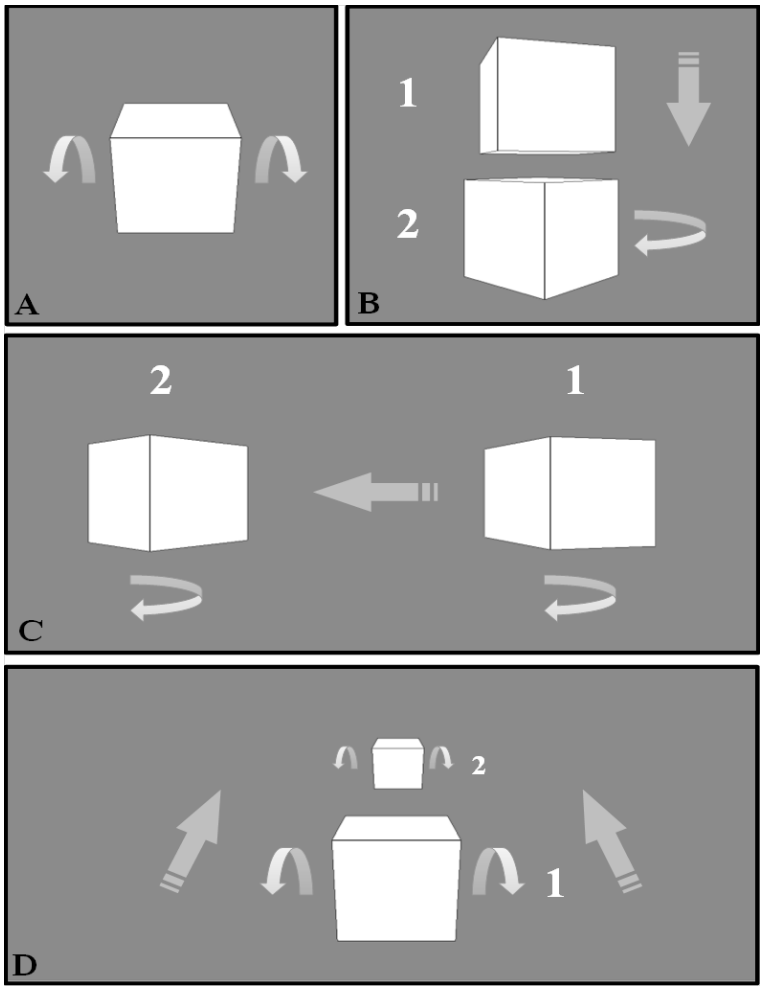

Figure 6-6 Combination of Motor Imagery and SSVEP in three different scenarios A) Pure Rotation B-D) Rotation and Translation around x , y and z axis.

In the first experiment, the cube rotates along the horizontal axis which passes its geometric center. In the second experiment, as the cube moves from the position of initial state 1 to that of final state 2, it also rotates about the vertical axis that passes its geometric center. The third experiment is similar to the second one, but

instead of translating from right to left, the cube goes from top to bottom. In the fourth experiment, the cube recedes into the screen along the axis that perpendicular to the screen and rotates along the horizontal axis that passes its geometric center at the same time.

6.2.3 SSVEP Detection

An SSVEP BCI reflects the user's attention to an oscillating visual stimulus. Let consider the EEG signal recorded at N_y channels in response to to a visual stimulation with a flicker frequency of f Hz. The SSVEP response recorded at each channel ($y_i(t)$) can be modeled as Equation 6-6.

$$y_i(t) = \sum_{n=1}^{N_h} \left[a_{in} \sin(2\pi nft) + b_{in} \cos(2\pi nft) \right] + E_i(t) \tag{6-6}$$

Equation 6-6 is a linear model which considers the dominant activity of N_h harmonics of the flickering frequency in terms of sine and cosine functions. Any other components including other non-SSVEP cognitive process, noise and artifacts are considered in the second part ($E_i(t)$). Equation 6-6 can be expressed in vector form as Equation 6-7.

$$y_i = Xg_i + E_i \tag{6-7}$$

where $y_i = [y_i(1) \quad \dots \quad y_i(N_t)]^T$ is the EEG of the i^{th} electrode containing N_t data points. X is the observation matrix which contains sine and cosine components of SSVEP response. The corresponding amplitude of matrix X, (a_{in} and b_{in}) are represented with Vector g_i. Equation 6-7 can be further generalized for N_y electrodes as Equation 6-8.

$$Y_{N_t \times N_y} = X_{N_t \times 2N_h} G_{2N_h \times N_y} + E_{N_t \times N_y} \quad (6\text{-}8)$$

where $Y = [y_1, \ldots, y_{Ny}]$ and $G = [g_1, \ldots, g_{Ny}]$ include all the EEG data points recorded at N_y channels and their associated harmonic amplitudes respectively.

In order to enhance the SSVEP component in the recorded signal, a virtual channel is defined as a linear combination of all the electrode signals, Y

$$s_{N_t \times 1} = Y_{N_T \times N_y} w_{N_y \times 1} \quad (6\text{-}9)$$

$w_{N_y \times 1}$ is a weighting vector corresponding to the contribution of each recorded signal in the enhanced signal. The weighting vector should is selected to minimize the non-SSVEP components. Therefore, a linear unbiased estimator is used to estimate and thus extract the SSVEP components from the recorded signals.

$$\tilde{Y} = Y - X(X^T X)^{-1} X^T Y \quad (6\text{-}10)$$

In Equation 6-10 the term $X(X^T X)^{-1} X^T Y$ is an estimate of SSVEP component and $\tilde{Y}$ is the remaining signal associated with noise, artifacts and background brain activity. The weighting vector W is then estimated such that it minimizes the energy of non-SSVEP component of the signal as shown in Equation 6-11:

$$\hat{w} = \arg\min \left\| \tilde{Y} \hat{w} \right\|^2 \quad (6\text{-}11)$$

Herrmann has shown that the minimal eigenvalue of matrix $\tilde{Y}^T \tilde{Y}$ will minimize the cost function in Equation 6-11 [137]. The weight matrix is hence chosen based on the minimum eigenvalue (λ_1) and its corresponding eigenvectors (v_1):

$$w_{N_y \times 1} = v_1 / \sqrt{\lambda_1} \quad (6\text{-}12)$$

In SSVEP based BCI applications, the stimulation frequency should be detected as a dominant frequency in the power spectral density. Hence, to detect the presence of a frequency in the spatially filtered signals, the ratio of power of the signal (PSD) at the target frequency with respect to the maximum power of the signal is calculated as shown in Equation 6-13.

$$R = \frac{\max\left[PSD(s)\,|_{f-0.1}^{f+0.1}\right]}{\max\left[PSD(s)\,|_{6}^{64}\right]} \tag{6-13}$$

The ratio of 1 shows that flashing frequency is dominant in the signal and therefore the SSVEP is detectable.

6.2.4 Results

A comparison between the power spectral density of the weighted signal calculated with Equation 6-16 and the signals recorded at different location near visual cortex are shown in Figure 6-7. In the actual system implementation, N_h = 2.

As it can be seen in Figure 6-7, the target frequency has a high power in the average signals of 40 trials; however it is undetectable in single trial recorded at each of the electrodes due to high activity in alpha frequency band (8-11 Hz). Finally it shows that the single trial of the weighted signal has its maximum power at the target frequency which clearly shows the effectiveness of weighting method.

Moreover, since our long-term goal is to use SSVEP as feedback to implement the motor imagery, we desire a high refresh rate of signal in the time domain. On the other hand, since the sampling rate of the signal is only 128 Hz, too short signal interval in time domain may cause failure to detect the SSVEP. Because of this trade-

off, a test on the accuracy of SSVEP detection was done by selecting moving windows of different length.

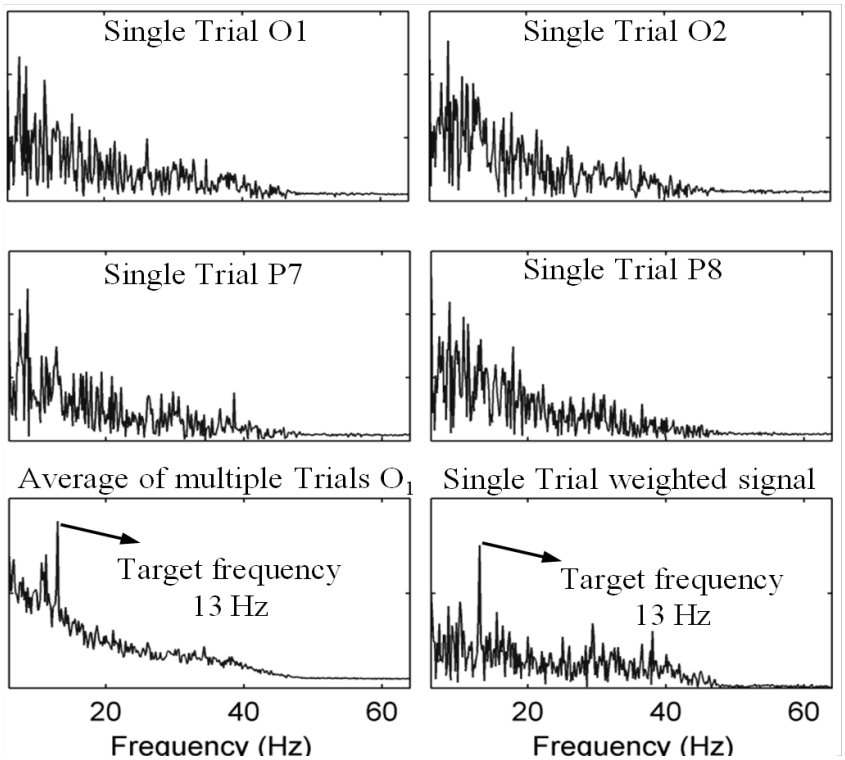

Figure 6-7 comparison between the power of target frequency in single trial signal of each electrode, the average and the weighted signal

Figure 6-8 shows the details of how moving windows are selected. L is the length of entire signal that recorded in the time domain. The first subset has length L_w which started from the initial time. Then the subset is modified by shifting forward of d seconds.

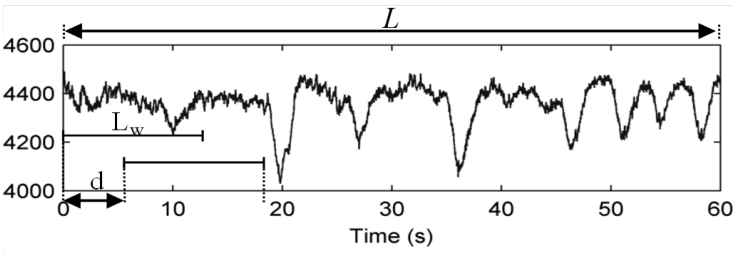

Figure 6-8 The parameters of moving window to be optimized

The averaged SSVEP detection rate over all subjects, for different values of L_w and d is illustrated in Figure 6-9. Each figure compares the classification rate with the control.

As it can be seen in Figure 6-9 the minimum classification rate appears at the smallest size of the moving window where the number of available data points is relatively low.

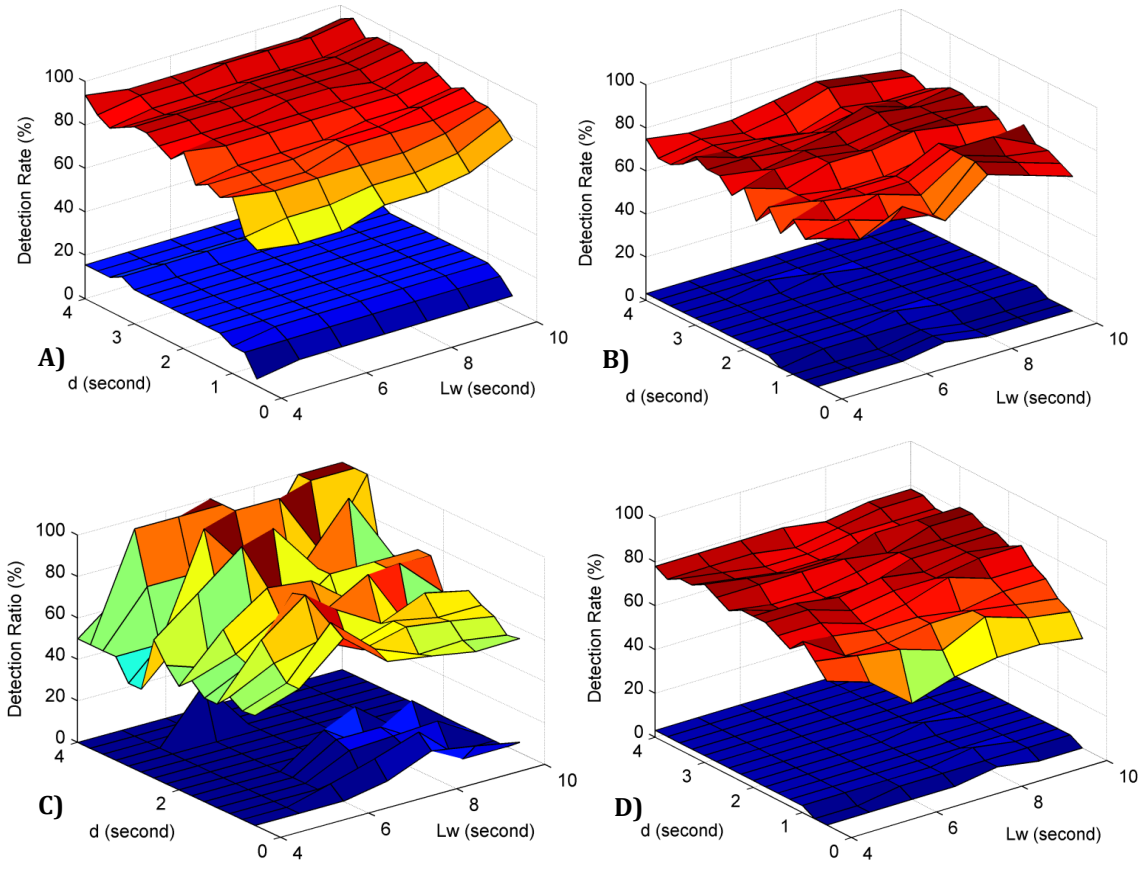

Figure 6-9 SSVEP detection rate for A) pure rotation-Exp 1A, B) rotation and translation x-axis-Exp 1B, C) rotation and translation y-axis -Exp 1C, D) rotation and translation z-axis -Exp 1D

The classification has to take the moment into account when the user does not focus on any stimuli. For this reason, the SSVEP detection rate in the normal condition is also calculated. The lower surfaces in Figure 6-9 show the SSVEP detection rate in normal condition or in other words the rate of false alarm in classification. In three out of four experiments, the average false alarm is less than 5%. Pure rotation with no flashing experiences the maximum misclassification of idle case as SSVEP. To further investigate the reason of false alarm and SSVEP misclassification, the normalized power of signal at flashing frequency is shown in Figure 6-10.

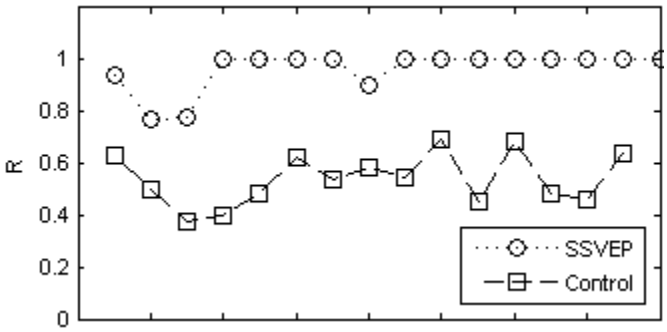

Figure 6-10 SSVEP detection rate for rotation and translation vs. normal condition

It is worth nothing that the stimulation frequency is located very close to the alpha band, this could produce false classifications in the resting state or slightly reduce the normalized power of the target frequency. In this case, the *R* value will be slightly less than one and still classify as non-SSVEP.

Such problems could easily be avoided by introducing a proper threshold for *R* value and/or using calibration session for every subject. In the calibration session, the power of the target frequency is normalized with respect to the normal

condition. However, the calibration session is avoided in this study to eliminate the training period of the SSVEP detection to consider the worst case scenario when it is used as brain switch in a hybrid BCI.

Chapter 7

Conclusion

This dissertation investigates the brain-computer interface, specifically the electroencephalogram (EEG), as an alternative user interface modality for computer-aided design (CAD) systems used in mechanical engineering. The goal of such a system is to enable designers to create and manipulate objects by imagining the geometric operations in their mind. Each chapter of the thesis focuses on a different application of BCI in CAD- specifically in object creation, object/surface selection and modification and user feedback by detecting the emotional state of the user.

7.1 Visual Imagery for geometry creation

Chapter 4 discussed experiments to explore object creation using visual imagery. The experiment required the subject imagine one of five primitive shapes. Features of interest were marginal spectrum of different frequency bands calculated from Hilbert spectrum of each independent component of EEG data. The results show an

average classification accuracy of 56.7% over seven subjects (ranging from 45 to 65%) using multi class LDA classifier.

Furthermore, the results were cross-validated by training and testing the classifier on data recorded with various stimuli (image and text) in different sessions. In this case, an average accuracy of 50.3% (range of 42-56%) was achieved over the entire subject. The fact that the classifier could maintain the classification accuracy over different modalities supports the finding of Suppes et al. [95] that showed invariance of brain-wave representation of visual image and their name.

This result indicates the potential of using BCI for distinguishing between primitive shapes. However, as the complexity of shape increases, generation and maintenance of visual objects becomes more difficult [87]. This means that classification of visual imagery using the above methods may be limited to very simple and primitive shapes and may not provide the CAD system the whole capability of object generation. However, the classification results of complex objects show a possible correlation between the features of the geometry (such as roundedness, sharpness, symmetry and curvature) and the extracted features of EEG signal. Capturing some of the main geometrical features of complex objects can provide the CAD system with information about the object that user intends to create or modify.

To investigate this matter, two binary classifiers were designed to distinguish between contrasting geometrical features (sharpness vs. roundness and parallel vs.

taper extrusion). The result showed an average classification rate of 69.8% for roundness vs. sharpness and 78.2% for parallel vs. tapered extrusion.

EEG signals rely heavily on careful manipulation of experimental conditions to minimize experimental confounds. Thus, many of the studies may be limited in generalizability. So for future work, the effect of other visual imagery characteristics, which were controlled in our study -such as color, texture or even size- should be studied. Furthermore, it would be necessary to conduct experiments in a more naturalistic setting.

Another interesting issue to investigate is the capability of BCI system in differentiation between imagery of positive and negative shapes which could enable the user to perform task similar to Boolean operations.

7.2 Satisfaction Detection

We investigated the feasibility of BCI to detect positive, negative or neutral human emotional responses to a machine's performance. Detection of the level of user satisfaction can provide a method to provide feedback to the classification algorithms and to modify the system behavior in response to user's response to the machine's actions.

Using the power spectral density and largest Lyapunov exponents, a classification rate of 79.2% was achieved by considering data recorded from all subjects. Furthermore, the accuracy of subject based emotional classification was

found to be much higher than the overall accuracy with using the same method (80.2%-94.7%).

Although the subject based classifier provides better accuracy, it needs separate training data for each individual user. Though the training period is not a significant problem for single user applications, it may not be practical in multi-user environments. Therefore, for future work, an adaptive classification method seems to be a wise choice as it can pre-trained based on emotional response of a large group of humans and then adapted as it interacts with a new user.

Another important point to consider is the difference in the source and level of frustration in human-human interaction with human-machine interaction. Thus in order to use the satisfaction level as a cognitive feedback, it is important to further investigate these differences and take them into account.

7.3 Object Selection with P300

In Chapter 6, we described an experiment and algorithms for using EEG based brain computer interfaces for selecting a target face in CAD environment. The experiment relied on evoking attention to rare stimuli in a random series of stimulus events (i.e., the oddball paradigm).

Discrete wavelet transform was the main tool for detecting the evoked P300 component. The coefficients of the DWT contain information in both time and frequency domains. Therefore, using them as the candidate features provided the classifier with information about changing frequency components in time.

The classification results show a promising application of BCI in CAD environments. In this experiment, we only considered a relatively simple geometry for face selection. However, to make the system more applicable, different geometries with different number of faces needs to be considered. Future work also needs to investigate whether the number of faces, their size and orientation introduce some limitation in face selection.

To further improve the accuracy of the classification, a proper method should be used to visually evoke the P300 component. This method should be able to adapt the flashing scheme based on the geometrical features of the object (e.g. number of flat faces, number of curved faces, and size of the faces). Finally the trade-off between the number of stimuli and the processing time should be carefully evaluated to avoid visual fatigue in subjects and to increase the information transfer rate.

7.4 Outlook for BCI applications in CAD

Brain–computer interfaces (BCIs) are recent developments in alternative technologies of human computer interaction. They promise a novel channel to engage human cognitive/emotional states in computer-aided systems. However, BCI applications in CAD/E systems are still in their early stages and thus further research and development are necessary to ensure that BCIs can meet the needs of specific user groups.

It has been recently suggested that the future generation of knowledge based CAD systems will be characterized by four features: “they will be based on cognitive

accounts of design, and they will support collaborative design, conceptual design, and creative design" [140]. Having this vision in mind, our outlook of BCI applications in CAD falls under the following three main categories:

1. Studying the neurological basis of design cognition :

Understanding designer's cognitive process during design activity plays a significant role in developing design theory and methodology. The first study to use brain's activity during design process was conducted by Göker in 1997 [141]. He studied the effect of experience in design process by analyzing the designer's EEG activity. His findings show that novice designers use deductive reasoning in design process while experts prefer to apply their experience directly.

Despite the importance of studying the design cognition, most of the research has been focused on other relative concepts such as creative thinking. Although design process is a creative task with its own flexibility, it also depends on a set of well-structured steps for analyzing the problem, finding and expressing the solution and finally evaluating the final design.

One future direction of research in this category of BCI application would be to develop metrics and methods to evaluate user's cognition during the early stage of design. The effects of parameters such as experience, creativity, familiarity with design team and even social skills on *selection* and *evaluation* process in design activity are particularly important.

2. Novel CAD/E applications for shape, structure, and product modeling or evaluation through brain-computer interfaces.

To the best of our knowledge, this dissertation is the first attempt to use BCI for product modeling and generation. However, from the human-computer interaction point of view, object creation or modeling is simply a transfer of information from user to the machine, which in case of BCI is in the form of a mental command. To completely replace the traditional mouse-keyboard interface, BCI or, any other alternative interface, should provide a competitive information transfer rate.

Despite the technological developments, there remain numerous obstacles to building efficient BCIs. The biggest challenges are related to accuracy and information transfer rate (ITR). The maximum ITR of current BCI systems is in the order of 35 bits/min for visual imagery [28], 55 bits/min for P300 based applications [142] and 124 bits/min for SSVEP [143].

This suggests that BCI may be better used as an additional modality during the process rather than a stand-alone mode of human-computer interaction. BCI can provide information that traditional mouse-keyboard, or even more recent modalities such as gesture and sketch-based systems cannot provide. The emotional and cognitive state of the user and the level of concentration are examples of information that BCIs can contribute in a multi-modal system. As an example for product modeling, the user can start creating the product using the traditional modalities, while his brain signal is being analyzed simultaneously. Using the visual imagery classification, BCI can detect the category of the object and/or some general geometrical features (e.g. symmetry) which will benefit the product design. Therefore, we envision that effective integration of BCI communication

with other modalities in design tools and systems would probably have a major impact in near future.

3. BCI system in collaborative conceptual design:

This category in fact is a combination of the two prior categories. The main direction of this research should be the implementation of concepts discovered in studying the design cognition in to a collaborative design environment where multiple users and machine interact.

Such applications can benefit from algorithms and methods in passive BCI systems such as the detection of workload or the emotional state of a user or the cognitive states involved in design collaboration.

References

[1] C. Tian, M. Masry, and H. Lipson, "Physical sketching: Reconstruction and analysis of 3D objects from freehand sketches," *Computer-Aided Design*, vol. 41, no. 3, pp. 147-158, Mar. 2009.

[2] S. Payandeh, J. Dill, and J. Zhang, "Using haptic feedback as an aid in the design of passive mechanisms," *Computer-Aided Design*, vol. 39, no. 6, pp. 528-538, Jun. 2007.

[3] X. Y. Kou, S. K. Xue, and S. T. Tan, "Knowledge-guided inference for voice-enabled CAD," *Computer-Aided Design*, vol. 42, no. 6, pp. 545-557, Jun. 2010.

[4] F. Amirouche, *Principles of Computer Aided Design and Manufacturing*, 2nd ed. Prentice Hall, 2004.

[5] A. Lecuyer, F. Lotte, R. B. Reilly, R. Leeb, M. Hirose, and M. Slater, "Brain-Computer Interfaces, virtual reality, and videogames," *Computer*, vol. 41, no. 10, pp. 66-72, Oct. 2008.

[6] R. Krepki, B. Blankertz, G. Curio, and K.-R. Müller, "The Berlin Brain-Computer Interface (BBCI) – towards a new communication channel for online control in gaming applications," *Multimedia Tools and Applications*, vol. 33, no. 1, pp. 73-90, Feb. 2007.

[7] G. Pfurtscheller et al., "Walking from thought.," *Brain research*, vol. 1071, no. 1, pp. 145-52, Feb. 2006.

[8] "www.emotiv.com".

[9] "http://www.neurosky.com".

[10] J. R. Wolpaw, N. Birbaumer, D. J. McFarland, G. Pfurtscheller, and T. M. Vaughan, "Brain–computer interfaces for communication and control," *Clinical Neurophysiology*, vol. 113, no. 6, pp. 767-791, Jun. 2002.

[11] T. O. Zander and C. Kothe, "Towards passive brain-computer interfaces: applying brain-computer interface technology to human-machine systems in general.," *Journal of neural engineering*, vol. 8, no. 2, p. 025005, Apr. 2011.

[12] S. Luck, *An Introduction to the Event-Related Potential Technique*. Cambridge, MA: MIT Press, 2005, p. 374.

[13] K. Jerbi et al., "Inferring hand movement kinematics from MEG, EEG and intracranial EEG: From brain-machine interfaces to motor rehabilitation," *IRBM*, vol. 32, no. 1, pp. 8-18, Feb. 2011.

[14] E. C. Leuthardt, K. J. Miller, G. Schalk, R. P. N. Rao, and J. G. Ojemann, "Electrocorticography-based brain computer interface-the Seattle experience.," *IEEE transactions on neural systems and rehabilitation engineering*, vol. 14, no. 2, pp. 194-8, Jun. 2006.

[15] J. A. Wilson, E. A. Felton, P. C. Garell, G. Schalk, and J. C. Williams, "ECoG factors underlying multimodal control of a brain-computer interface.," *IEEE transactions on neural systems and rehabilitation engineering*, vol. 14, no. 2, pp. 246-50, Jun. 2006.

[16] L. R. Hochberg et al., "Neuronal ensemble control of prosthetic devices by a human with tetraplegia.," *Nature*, vol. 442, no. 7099, pp. 164-71, Jul. 2006.

[17] M. E. Raichle, "A brief history of human brain mapping.," *Trends in neurosciences*, vol. 32, no. 2, pp. 118-26, Feb. 2009.

[18] N. Weiskopf et al., "Principles of a brain-computer interface (BCI) based on real-time functional magnetic resonance imaging (fMRI).," *IEEE transactions on bio-medical engineering*, vol. 51, no. 6, pp. 966-70, Jun. 2004.

[19] S. D. Newman, R. L. Klatzky, S. J. Lederman, and M. A. Just, "Imagining material versus geometric properties of objects: an fMRI study.," *Brain research. Cognitive brain research*, vol. 23, no. 2–3, pp. 235-46, May 2005.

[20] A. Guillot, C. Collet, V. A. Nguyen, F. Malouin, C. Richards, and J. Doyon, "Brain activity during visual versus kinesthetic imagery: an fMRI study.," *Human brain mapping*, vol. 30, no. 7, pp. 2157-72, Jul. 2009.

[21] M. M. Ter-Pogossian, M. E. Phelps, E. J. Hoffman, and N. A. Mullani, "A positron-emission transaxial tomograph for nuclear imaging (PETT).," *Radiology*, vol. 114, no. 1, pp. 89-98, Jan. 1975.

[22] R. Sitaram et al., "Temporal classification of multichannel near-infrared spectroscopy signals of motor imagery for developing a brain-computer interface.," *NeuroImage*, vol. 34, no. 4, pp. 1416-27, Feb. 2007.

[23] B. Chance et al., "A novel method for fast imaging of brain function, non-invasively, with light," *Optics Express*, vol. 2, no. 10, p. 411, May 1998.

[24] T. O. Zander, C. Kothe, S. Jatzev, and M. Gaertner, "Enhancing Human-Computer Interaction with Input from Active and Passive Brain-Computer Interfaces," in *Brain-Computer Interfaces Applying our Minds to Human-Computer Interaction*, D. S. Tan and A. Nijholt, Eds. London: Springer London, 2010, pp. 181-199.

[25] G. Townsend, B. Graimann, G. Pfurtscheller, and A. Nearly, "Continuous EEG Classification During Motor Imagery — Simulation of an Asynchronous BCI," vol. 12, no. 2, pp. 258-265, 2004.

[26] T. Quang, D. Khoa, N. Yuichi, and N. Masahiro, "Chaos , Solitons and Fractals Recognizing brain motor imagery activities by identifying chaos properties of oxy-hemoglobin dynamics time series," *Chaos, Solitons and Fractals*, vol. 42, no. 1, pp. 422-429, 2009.

[27] P. Herman, G. Prasad, S. Member, T. M. Mcginnity, and D. Coyle, "Comparative Analysis of Spectral Approaches to Feature Extraction for EEG-Based Motor Imagery Classification," vol. 16, no. 4, pp. 317-326, 2008.

[28] P. Bobrov, A. Frolov, C. Cantor, I. Fedulova, M. Bakhnyan, and A. Zhavoronkov, "Brain-computer interface based on generation of visual images.," *PloS one*, vol. 6, no. 6, p. e20674, Jan. 2011.

[29] E. T. Esfahani and V. Sundararajan, "Classification of primitive shapes using brain–computer interfaces," *Computer-Aided Design*, vol. 44, no. 10, pp. 1011-1019, May 2012.

[30] E. Curran et al., "Cognitive tasks for driving a brain-computer interfacing system: a pilot study.," *IEEE transactions on neural systems and rehabilitation engineering*, vol. 12, no. 1, pp. 48-54, Mar. 2004.

[31] G. Pfurtscheller and C. Neuper, "Motor imagery and direct brain-computer communication," *Proceedings of the IEEE*, vol. 89, no. 7, pp. 1123-1134, Jul. 2001.

[32] E. Curran, "Learning to control brain activity: A review of the production and control of EEG components for driving brain–computer interface (BCI) systems," *Brain and Cognition*, vol. 51, no. 3, pp. 326-336, Apr. 2003.

[33] L. Fabien, L. Anatole, L. Fabrice, and A. Bruno, "Studying the use of fuzzy inference systems for motor imagery classification.," *IEEE transactions on neural systems and rehabilitation engineering*, vol. 15, no. 2, pp. 322-4, Jun. 2007.

[34] F. Babiloni et al., "Linear classification of low-resolution EEG patterns produced by imagined hand movements.," *IEEE transactions on rehabilitation engineering*, vol. 8, no. 2, pp. 186-8, Jun. 2000.

[35] H. Yuan, C. Perdoni, and B. He, "Relationship between speed and EEG activity during imagined and executed hand movements.," *Journal of neural engineering*, vol. 7, no. 2, p. 26001, Apr. 2010.

[36] A. Schlögl, F. Lee, H. Bischof, and G. Pfurtscheller, "Characterization of four-class motor imagery EEG data for the BCI-competition 2005.," *Journal of neural engineering*, vol. 2, no. 4, pp. L14-22, Dec. 2005.

[37] G. Pfurtscheller et al., "15 years of BCI research at Graz University of Technology: current projects.," *IEEE transactions on neural systems and rehabilitation engineering*, vol. 14, no. 2, pp. 205-10, Jun. 2006.

[38] J. J. Daly and J. R. Wolpaw, "Brain-computer interfaces in neurological rehabilitation.," *Lancet neurology*, vol. 7, no. 11, pp. 1032-43, Nov. 2008.

[39] A. Martin, "The Representation of object concepts in the brain.," *Annual Review of Psychology*, vol. 58, pp. 25-45, 2007.

[40] L. Reddy, N. Tsuchiya, and T. Serre, "Reading the mind's eye: decoding category information during mental imagery.," *NeuroImage*, vol. 50, no. 2, pp. 818-25, Apr. 2010.

[41] I. Simanova, M. van Gerven, R. Oostenveld, and P. Hagoort, "Identifying object categories from event-related EEG: toward decoding of conceptual representations.," *PloS one*, vol. 5, no. 12, p. e14465, Jan. 2010.

[42] E. Donchin, K. M. Spencer, and R. Wijesinghe, "The mental prosthesis: assessing the speed of a P300-based brain-computer interface," *IEEE Transactions on Rehabilitation Engineering*, vol. 8, no. 2, pp. 174-179, Jun. 2000.

[43] W. Speier, C. Arnold, J. Lu, R. K. Taira, and N. Pouratian, "Natural language processing with dynamic classification improves P300 speller accuracy and bit rate.," *Journal of neural engineering*, vol. 9, no. 1, p. 016004, Feb. 2012.

[44] S. P. Kelly, E. C. Lalor, R. B. Reilly, S. Member, and J. J. Foxe, "High-Density SSVEP Data for Independent Brain – Computer Communication," vol. 13, no. 2, pp. 172-178, 2005.

[45] E. C. Lalor et al., "Steady-State VEP-Based Brain-Computer Interface Control in an Immersive 3D Gaming Environment," *EURASIP Journal on Advances in Signal Processing*, vol. 2005, no. 19, pp. 3156-3164, 2005.

[46] D. Zhu, J. Bieger, G. Garcia Molina, and R. M. Aarts, "A survey of stimulation methods used in SSVEP-based BCIs.," *Computational intelligence and neuroscience*, vol. 2010, pp. 1-12, Jan. 2010.

[47] G. R. Müller-Putz, R. Scherer, C. Neuper, and G. Pfurtscheller, "Steady-state somatosensory evoked potentials: suitable brain signals for brain-computer interfaces?," *IEEE transactions on neural systems and rehabilitation engineering*, vol. 14, no. 1, pp. 30-7, Mar. 2006.

[48] C. Breitwieser, V. Kaiser, C. Neuper, and G. R. Müller-Putz, "Stability and distribution of steady-state somatosensory evoked potentials elicited by vibro-tactile stimulation.," *Medical & biological engineering & computing*, vol. 50, no. 4, pp. 347-57, Apr. 2012.

[49] M. a. Lopez-Gordo, F. Pelayo, a. Prieto, and E. Fernandez, "an Auditory Brain-Computer Interface With Accuracy Prediction," *International Journal of Neural Systems*, vol. 22, no. 03, pp. 1250009-1, 2012.

[50] F. Nijboer et al., "A P300-based brain-computer interface for people with amyotrophic lateral sclerosis.," *Clinical neurophysiology*, vol. 119, no. 8, pp. 1909-16, Aug. 2008.

[51] L. A. Farwell and E. Donchin, "Talking off the top of your head: toward a mental prosthesis utilizing event-related brain potentials.," *Electroencephalography and clinical neurophysiology*, vol. 70, no. 6, pp. 510-23, Dec. 1988.

[52] M. Cheng, X. Gao, S. Gao, and D. Xu, "Design and implementation of a brain-computer interface with high transfer rates.," *IEEE transactions on bio-medical engineering*, vol. 49, no. 10, pp. 1181-6, Oct. 2002.

[53] C.-H. Wu et al., "Frequency recognition in an SSVEP-based brain computer interface using empirical mode decomposition and refined generalized zero-crossing.," *Journal of neuroscience methods*, vol. 196, no. 1, pp. 170-81, Mar. 2011.

[54] R. Ortner, B. Z. Allison, G. Korisek, H. Gaggl, and G. Pfurtscheller, "An SSVEP BCI to control a hand orthosis for persons with tetraplegia.," *IEEE transactions on neural systems and rehabilitation engineering*, vol. 19, no. 1, pp. 1-5, Feb. 2011.

[55] I. Volosyak, "SSVEP-based Bremen-BCI interface--boosting information transfer rates.," *Journal of neural engineering*, vol. 8, no. 3, p. 036020, Jun. 2011.

[56] C. Berka et al., "EEG correlates of task engagement and mental workload in vigilance, learning, and memory tasks.," *Aviation, space, and environmental medicine*, vol. 78, no. 5 Suppl, pp. B231-44, May 2007.

[57] R. Parasuraman and G. F. Wilson, "Putting the brain to work: neuroergonomics past, present, and future.," *Human factors*, vol. 50, no. 3, pp. 468-74, Jun. 2008.

[58] M. Y. V. Bekkedal, J. Rossi, and J. Panksepp, "Human brain EEG indices of emotions: delineating responses to affective vocalizations by measuring frontal theta event-related synchronization.," *Neuroscience and biobehavioral reviews*, vol. 35, no. 9, pp. 1959-70, Oct. 2011.

[59] R. Chavarriaga and J. D. R. Millan, "Learning from EEG error-related potentials in noninvasive brain-computer interfaces.," *IEEE transactions on neural systems and rehabilitation engineering*, vol. 18, no. 4, pp. 381-8, Aug. 2010.

[60] E. M. Ventouras, P. Asvestas, I. Karanasiou, and G. K. Matsopoulos, "Classification of Error-Related Negativity (ERN) and Positivity (Pe) potentials using kNN and Support Vector Machines.," *Computers in biology and medicine*, vol. 41, no. 2, pp. 98-109, Feb. 2011.

[61] P. W. Ferrez and J. del R Millan, "Error-related EEG potentials generated during simulated brain-computer interaction.," *IEEE transactions on bio-medical engineering*, vol. 55, no. 3, pp. 923-9, Mar. 2008.

[62] J. Onton and S. Makeig, "Information-based modeling of event-related brain dynamics.," *Progress in brain research*, vol. 159, pp. 99-120, Jan. 2006.

[63] a J. Bell and T. J. Sejnowski, "An information-maximization approach to blind separation and blind deconvolution.," *Neural computation*, vol. 7, no. 6, pp. 1129-59, Nov. 1995.

[64] S. Amari, A. Cichocki, and H. H. Yang, "A New Learning Algorithm for Blind Signal Separation," in *Advances in neural information processing systems*, D. Touretzky, M. Mozer, and M. Hasselmo, Eds. MIT Press, 1996, pp. 757–763.

[65] A. Delorme and S. Makeig, "EEGLAB: an open source toolbox for analysis of single-trial EEG dynamics including independent component analysis.," *Journal of neuroscience methods*, vol. 134, no. 1, pp. 9-21, Mar. 2004.

[66] T. P. Jung et al., "Removing electroencephalographic artifacts by blind source separation.," *Psychophysiology*, vol. 37, no. 2, pp. 163-78, Mar. 2000.

[67] J. O. B. P. Lindsen and J. Bhattacharya, "Correction of blink artifacts using independent component analysis and empirical mode decomposition.," *Psychophysiology*, vol. 47, no. 5, pp. 955-60, Sep. 2010.

[68] D. L. Schomer, "The Normal EEG in an Adult," in *The clinical neurophysiology primer*, A. S. Blum and S. B. Rutkove, Eds. Humana Press, 2007, pp. 57-71.

[69] F. Lotte and M. Congedo, "A review of classification algorithms for EEG-based brain – computer interfaces," vol. 1, 2007.

[70] N. J. Thomas, "Mental Imagery," *The Stanford Encyclopedia of Philosophy*, 2011. .

[71] S. Kosslyn and D. Osherson, Eds., "Mental Imagery," in *Visual Cognition: An Invitation to Cognitive Science*, 2nd ed., MIT Press, 1995, pp. 267-296.

[72] S. T. Moulton and S. M. Kosslyn, "Imagining predictions: mental imagery as mental emulation.," *Philosophical transactions of the Royal Society of London. Series B, Biological sciences*, vol. 364, no. 1521, pp. 1273-80, May 2009.

[73] C. Brunner, M. Naeem, R. Leeb, B. Graimann, and G. Pfurtscheller, "Spatial filtering and selection of optimized components in four class motor imagery EEG data using independent components analysis," *Pattern Recognition Letters*, vol. 28, no. 8, pp. 957-964, Jun. 2007.

[74] A. Kübler, B. Kotchoubey, J. Kaiser, J. R. Wolpaw, and N. Birbaumer, "Brain-computer communication: Unlocking the locked in.," *Psychological Bulletin*, vol. 127, no. 3, pp. 358-375, 2001.

[75] S. Lemm, C. Schäfer, and G. Curio, "BCI Competition 2003--Data set III: probabilistic modeling of sensorimotor mu rhythms for classification of imaginary hand movements.," *IEEE transactions on bio-medical engineering*, vol. 51, no. 6, pp. 1077-80, Jun. 2004.

[76] J. D. R. Millán and J. Mouriño, "Asynchronous BCI and local neural classifiers: an overview of the Adaptive Brain Interface project.," *IEEE transactions on neural systems and rehabilitation engineering*, vol. 11, no. 2, pp. 159-61, Jun. 2003.

[77] G. E. Fabiani, D. J. McFarland, J. R. Wolpaw, and G. Pfurtscheller, "Conversion of EEG activity into cursor movement by a brain-computer interface (BCI).," *IEEE transactions on neural systems and rehabilitation engineering*, vol. 12, no. 3, pp. 331-8, Sep. 2004.

[78] L. J. Trejo, R. Rosipal, and B. Matthews, "Brain-computer interfaces for 1-D and 2-D cursor control: designs using volitional control of the EEG spectrum or steady-state visual evoked potentials.," *IEEE transactions on neural systems and rehabilitation engineering*, vol. 14, no. 2, pp. 225-9, Jun. 2006.

[79] A. R. Nikolaev, "Investigation of the stages of the mental rotation of complex figures with the intracortical interaction mapping technique," *Neuroscience and Behavioral Physiology*, vol. 25, no. 3, pp. 228-233, May 1995.

[80] J. Martinovic, T. Gruber, and M. M. Müller, "Induced gamma band responses predict recognition delays during object identification.," *Journal of cognitive neuroscience*, vol. 19, no. 6, pp. 921-34, Jun. 2007.

[81] M. Kozhevnikov, S. Kosslyn, and J. Shephard, "Spatial versus object visualizers: a new characterization of visual cognitive style.," *Memory & cognition*, vol. 33, no. 4, pp. 710-26, Jun. 2005.

[82] M. J. Farah, K. M. Hammond, D. N. Levine, and R. Calvanio, "Visual and spatial mental imagery: dissociable systems of representation.," *Cognitive psychology*, vol. 20, no. 4, pp. 439-62, Oct. 1988.

[83] S. M. Kosslyn, "Mental images and the Brain.," *Cognitive neuropsychology*, vol. 22, no. 3, pp. 333-47, May 2005.

[84] M. D'Esposito et al., "A functional MRI study of mental image generation," *Neuropsychologia*, vol. 35, no. 5, pp. 725-730, Apr. 1997.

[85] E. Mellet, N. Tzourio, M. Denis, and B. Mazoyer, "A Positron Emission Tomography Study of Visual and Mental Spatial Exploration," *Journal of Cognitive Neuroscience*, vol. 7, no. 4, pp. 433-445, Oct. 1995.

[86] C. Cornoldi, R. D. Beni, A. Cavedon, G. Mazzoni, F. Giusberti, and F. Marucci, "How can a vivid image be described? Characteristics influencing vividness judgments and relationship between vividness and memory," *Journal of mental Imagery*, vol. 16, no. 3–4, pp. 89-108, 1992.

[87] D. Pearson, R. D. Beni, and C. Cornoldi, "The generation, maintenance, and transformation of visuo-spatial mental image," in *Imagery, language and visuo-spatial thinking*, M. Denis, R. Logie, C. Cornoldi, M. De Vega, and J. Engelkamp, Eds. Psychology Press Ltd., 2001, pp. 1-23.

[88] C. Koch and T. Poggio, "Predicting the visual world: silence is golden.," *Nature neuroscience*, vol. 2, no. 1, pp. 9-10, Jan. 1999.

[89] G. Pfurtscheller, C. Neuper, D. Flotzinger, and M. Pregenzer, "EEG-based discrimination between imagination of right and left hand movement," *Electroencephalography and Clinical Neurophysiology*, vol. 103, no. 6, pp. 642-651, Dec. 1997.

[90] G. Pfurtscheller, C. Neuper, A. Schlogl, and K. Lugger, "Separability of EEG signals recorded during right and left motor imagery using adaptive autoregressive parameters," *IEEE Transactions on Rehabilitation Engineering*, vol. 6, no. 3, pp. 316-325, Sep. 1998.

[91] T. Wang, J. Deng, and B. He, "Classifying EEG-based motor imagery tasks by means of time-frequency synthesized spatial patterns.," *Clinical neurophysiology*, vol. 115, no. 12, pp. 2744-53, Dec. 2004.

[92] N. Huang and S. Shen, *The Hilbert-Huang Transform in Engineering*. World Scientific Publishing Company, 2005.

[93] I. Biederman, "Recognition-by-components: a theory of human image understanding.," *Psychological review*, vol. 94, no. 2, pp. 115-47, Apr. 1987.

[94] I. Biederman, "Recognizing depth-rotated objects: a review of recent research and theory.," *Spatial vision*, vol. 13, no. 2–3, pp. 241-53, Jan. 2000.

[95] P. Suppes, "Invariance of brain-wave representations of simple visual images and their names," *Proceedings of the National Academy of Sciences*, vol. 96, no. 25, pp. 14658-14663, Dec. 1999.

[96] K.-robert Müller, C. W. Anderson, and G. E. Birch, "Linear and nonlinear methods for brain-computer interfaces.," *IEEE transactions on neural systems and rehabilitation engineering*, vol. 11, no. 2, pp. 165-9, Jun. 2003.

[97] K.-E. Ko, H.-C. Yang, and K.-B. Sim, "Emotion recognition using EEG signals with relative power values and Bayesian network," *International Journal of Control, Automation and Systems*, vol. 7, no. 5, pp. 865-870, Oct. 2009.

[98] P. C. Petrantonakis and L. J. Hadjileontiadis, "Emotion recognition from EEG using higher order crossings.," *IEEE transactions on information technology in biomedicine*, vol. 14, no. 2, pp. 186-97, Mar. 2010.

[99] M. Li and B.-L. Lu, "Emotion classification based on gamma-band EEG.," in *International Conference of the IEEE Engineering in Medicine and Biology Society*, 2009, pp. 1323-6.

[100] E. T. Esfahani and V. Sundararajan, "Using Brain-Computer Interfaces to Detec Human Datisfaction in Human-Robot Interactions," *International Journal of Humanoid Robotics*, vol. 08, no. 01, p. 87, 2011.

[101] K. Scherer, "Vocal communication of emotion: A review of research paradigms," *Speech Communication*, vol. 40, no. 1–2, pp. 227-256, Apr. 2003.

[102] T. Waaramaa, A.-M. Laukkanen, M. Airas, and P. Alku, "Perception of emotional valences and activity levels from vowel segments of continuous speech.," *Journal of voice : official journal of the Voice Foundation*, vol. 24, no. 1, pp. 30-8, Jan. 2010.

[103] B. Yang and M. Lugger, "Emotion recognition from speech signals using new harmony features," *Signal Processing*, vol. 90, no. 5, pp. 1415-1423, May 2010.

[104] L. Devillers, L. Vidrascu, and L. Lamel, "Challenges in real-life emotion annotation and machine learning based detection.," *Neural networks*, vol. 18, no. 4, pp. 407-22, May 2005.

[105] M. Pantie and L. J. M. Rothkrantz, "Automatic analysis of facial expressions: the state of the art," *IEEE Transactions on Pattern Analysis and Machine Intelligence*, vol. 22, no. 12, pp. 1424-1445, 2000.

[106] M. Pantic and L. J. . Rothkrantz, "Expert system for automatic analysis of facial expressions," *Image and Vision Computing*, vol. 18, no. 11, pp. 881-905, Aug. 2000.

[107] J. Anttonen and V. Surakka, "Emotions and heart rate while sitting on a chair," in *Proceedings of the SIGCHI conference on Human factors in computing systems*, 2005, p. 491.

[108] K. H. Kim, S. W. Bang, and S. R. Kim, "Emotion recognition system using short-term monitoring of physiological signals.," *Medical & biological engineering & computing*, vol. 42, no. 3, pp. 419-27, May 2004.

[109] J. A. Coan and J. J. B. Allen, "Frontal EEG asymmetry as a moderator and mediator of emotion.," *Biological psychology*, vol. 67, no. 1–2, pp. 7-49, Oct. 2004.

[110] S. K. Sutton and R. J. Davidson, "Prefrontal Brain Asymmetry: A Biological Substrate of the Behavioral Approach and Inhibition Systems," *Psychological Science*, vol. 8, no. 3, pp. 204-210, May 1997.

[111] Q. Zhang and M. Lee, "Analysis of positive and negative emotions in natural scene using brain activity and GIST," *Neurocomputing*, vol. 72, no. 4–6, pp. 1302-1306, Jan. 2009.

[112] K. Schaaff and T. Schultz, "Towards an EEG-based emotion recognizer for humanoid robots," *8th IEEE International Symposium on Robot and Human Interactive Communication*, pp. 792-796, Sep. 2009.

[113] C. a Frantzidis et al., "On the classification of emotional biosignals evoked while viewing affective pictures: an integrated data-mining-based approach for healthcare applications.," *IEEE transactions on information technology in biomedicine*, vol. 14, no. 2, pp. 309-18, Mar. 2010.

[114] R. J. Davidson, P. Ekman, C. D. Saron, J. a Senulis, and W. V. Friesen, "Approach-withdrawal and cerebral asymmetry: emotional expression and brain physiology. I.," *Journal of personality and social psychology*, vol. 58, no. 2, pp. 330-41, Feb. 1990.

[115] M. B. Kostyunina and M. A. Kulikov, "Frequency characteristics of EEG spectra in the emotions," *Neuroscience and Behavioral Physiology*, vol. 26, no. 4, pp. 340-343, Jul. 1996.

[116] L. Zhang, W. He, C. He, and P. Wang, "Improving Mental Task Classification by Adding High Frequency Band Information," *Journal of Medical Systems*, vol. 34, no. 1, pp. 51-60, Oct. 2008.

[117] C. Stam, *Nonlinear Brain Dynamics*. Nova Biomedical Publication, 2004.

[118] K. Natarajan, R. Acharya U, F. Alias, T. Tiboleng, and S. K. Puthusserypady, "Nonlinear analysis of EEG signals at different mental states.," *Biomedical engineering online*, vol. 3, no. 1, p. 7, Mar. 2004.

[119] X. Li, Z. Deng, and J. Zhang, "Function of EEG Temporal Complexity Analysis in Neural Activities Measurement," *Advances in Neural Networks*, vol. 5551, pp. 209-218, 2009.

[120] N. Packard, J. Crutchfield, J. Farmer, and R. Shaw, "Geometry from a Time Series," *Physical Review Letters*, vol. 45, no. 9, pp. 712-716, Sep. 1980.

[121] A. Wolf, J. B. Swift, H. L. Swinney, and J. A. Vastano, "Determining Lyapunov Exponents from a Time Series," *Physica D: Nonlinear Phenomena*, vol. 16, no. 3, pp. 285-317, 1985.

[122] C. Merkwirth, U. Parlitz, I.Wedekind, D. Engster, and W. Lauterborn, "OpenTSTOOL," 2009. [Online]. Available: URL:http://www.dpi.physik.uni-goettingen.de/tstool/.

[123] N. Xu, X. Gao, B. Hong, X. Miao, S. Gao, and F. Yang, "BCI Competition 2003--Data set IIb: enhancing P300 wave detection using ICA-based subspace projections for BCI applications.," *IEEE transactions on bio-medical engineering*, vol. 51, no. 6, pp. 1067-72, Jun. 2004.

[124] U. Hoffmann, J.-M. Vesin, T. Ebrahimi, and K. Diserens, "An efficient P300-based brain-computer interface for disabled subjects.," *Journal of neuroscience methods*, vol. 167, no. 1, pp. 115-25, Jan. 2008.

[125] A. Campbell et al., "NeuroPhone: brain-mobile phone interface using a wireless EEG headset," in *Proceedings of the second ACM SIGCOMM workshop on Networking, systems, and applications on mobile handhelds - MobiHeld '10*, 2010, pp. 3-8.

[126] A. Pinsky, *Introduction to Fourier Analysis and Wavelets*. American Mathematical Society, 2009.

[127] V. Abootalebi, M. H. Moradi, and M. A. Khalilzadeh, "A comparison of methods for ERP assessment in a P300-based GKT.," *International journal of psychophysiology*, vol. 62, no. 2, pp. 309-20, Nov. 2006.

[128] V. Abootalebi, M. H. Moradi, and M. A. Khalilzadeh, "A new approach for EEF feature extraction in P300-based lie detection.," *Computer Methods and Programs in Biomedicine*, vol. 94, no.1, pp.48-57, 2009.

[129] J. N. Mak and J. R. Wolpaw, "Clinical Applications of Brain-Computer Interfaces: Current State and Future Prospects.," *IEEE reviews in biomedical engineering*, vol. 2, pp. 187-199, Jan. 2009.

[130] G. Pfurtscheller and F. H. Lopes da Silva, "Event-related EEG/MEG synchronization and desynchronization: basic principles.," *Clinical neurophysiology*, vol. 110, no. 11, pp. 1842-57, Nov. 1999.

[131] J. Long, Y. Li, T. Yu, and Z. Gu, "Target selection with hybrid feature for BCI-based 2-D cursor control.," *IEEE transactions on bio-medical engineering*, vol. 59, no. 1, pp. 132-40, Jan. 2012.

[132] A. Kubler and K. Muller, "An introduction to brain–computer interfacing," in *Toward Brain–Computer Interfacing*, G. Dornhedge, J. Millan, T. Hinterberger, D. McFarland, and K. Muller, Eds. MIT Press, 2007, pp. 1-25.

[133] B. Z. Allison, C. Brunner, V. Kaiser, G. R. Müller-Putz, C. Neuper, and G. Pfurtscheller, "Toward a hybrid brain-computer interface based on imagined movement and visual attention.," *Journal of neural engineering*, vol. 7, no. 2, p. 26007, Apr. 2010.

[134] G. Pfurtscheller, T. Solis-Escalante, R. Ortner, P. Linortner, and G. R. Müller-Putz, "Self-paced operation of an SSVEP-Based orthosis with and without an imagery-based 'brain switch:' a feasibility study towards a hybrid BCI.," *IEEE transactions on neural systems and rehabilitation engineering*, vol. 18, no. 4, pp. 409-14, Aug. 2010.

[135] J. J. Vidal, "Real-time detection of brain events in EEG," *Proceedings of the IEEE*, vol. 65, no. 5, pp. 633-641, 1977.

[136] Y. Wang, X. Gao, B. Hong, C. Jia, and S. Gao, "Brain-computer interfaces based on visual evoked potentials.," *IEEE engineering in medicine and biology magazine*, vol. 27, no. 5, pp. 64-71, 2008.

[137] C. S. Herrmann, "Human EEG responses to 1-100Hz flicker: resonance phenomena in visual cortex and their potential correlation to cognitive phenomena," *Experimental Brain Research*, vol. 137, no. 3–4, pp. 346-353, Apr. 2001.

[138] P. F. Diez, V. A. Mut, E. M. Avila Perona, and E. Laciar Leber, "Asynchronous BCI control using high-frequency SSVEP.," *Journal of neuroengineering and rehabilitation*, vol. 8, p. 39, Jan. 2011.

[139] O. Friman, I. Volosyak, and A. Gräser, "Multiple channel detection of steady-state visual evoked potentials for brain-computer interfaces.," *IEEE transactions on bio-medical engineering*, vol. 54, no. 4, pp. 742-50, Apr. 2007.

[140] A. K. Goel, S. Vattam, B. Wiltgen and M. Helms "Cognitive, collaborative, conceptual and creative – Four characteristics of the next generation of knowledge-based CAD systems: A study in biologically inspired design," *Computer-Aided Design*, vol. 44, no. 10, pp. 879-900, 2012.

[141] M. Goker, "The effects of experience during design problem solving," *Design Studies*, vol. 18, no. 4, pp. 405-426, 1997.

[142] S. T. Ahi, H. Kambara, and Y. Koike, "A dictionary-driven P300 speller with a modifies interface.," *IEEE transactions on neural systems and rehabilitation engineering*, vol. 19, no. 1, pp. 6-14, 2011.

[143] I. Volosyak, "SSVEP-based Bremen-BCI interface--boosting information transfer rates.," *Journal of neural engineering*, vol. 8, no. 3, p. 036020, Jun. 2011